AD-A251 844

ivision
ce Warfare Center
-5000

CDNSWC–92/004 April 1992
Propulsion and Auxiliary Systems Department
Research and Development Report

DTIC
ELECTE
JUN 1 0 1992
S D
C

Propulsive Efficiencies of Magnetohydrodynamic Propulsors Considering Electrical and Magnetic End Effects

by
Paul A. Beatty
University of Vermont
Burlington, Vermont 05405

William F. Hughes
Carnegie Mellon University
Pittsburgh, Pennsylvania 15213

Samuel H. Brown, Joseph D. Walters, Neal A. Sondergaard,
and Howard O. Stevens
Naval Surface Warfare Center

92-15103

CDNSWC–92/004 Propulsive Efficiencies of Magnetohydrodynamic Propulsors Considering Electrical and Magnetic End Effects

Approved for public release; distribution is unlimited.

92 6 09 010

MAJOR DTRC TECHNICAL COMPONENTS

CODE 011 DIRECTOR OF TECHNOLOGY, PLANS AND ASSESSMENT

12 SHIP SYSTEMS INTEGRATION DEPARTMENT

14 SHIP ELECTROMAGNETIC SIGNATURES DEPARTMENT

15 SHIP HYDROMECHANICS DEPARTMENT

16 AVIATION DEPARTMENT

17 SHIP STRUCTURES AND PROTECTION DEPARTMENT

18 COMPUTATION, MATHEMATICS & LOGISTICS DEPARTMENT

19 SHIP ACOUSTICS DEPARTMENT

27 PROPULSION AND AUXILIARY SYSTEMS DEPARTMENT

28 SHIP MATERIALS ENGINEERING DEPARTMENT

DTRC ISSUES THREE TYPES OF REPORTS:

1. **DTRC reports, a formal series,** contain information of permanent technical value. They carry a consecutive numerical identification regardless of their classification or the originating department.

2. **Departmental reports, a semiformal series,** contain information of a preliminary, temporary, or proprietary nature or of limited interest or significance. They carry a departmental alphanumerical identification.

3. **Technical memoranda, an informal series,** contain technical documentation of limited use and interest. They are primarily working papers intended for internal use. They carry an identifying number which indicates their type and the numerical code of the originating department. Any distribution outside DTRC must be approved by the head of the originating department on a case-by-case basis.

NDW-DTNSRDC 5602/51 (Rev 2-88)

Carderock Division
Naval Surface Warfare Center
Bethesda, MD 20084–5000

CDNSWC–92/004 April 1992
Propulsion and Auxiliary Systems Department
Research and Development Report

Propulsive Efficiencies of Magnetohydrodynamic Propulsors Considering Electrical and Magnetic End Effects

by
Paul A. Beatty
University of Vermont
Burlington, Vermont 05405

William F. Hughes
Carnegie Mellon University
Pittsburgh, Pennsylvania 15213

Samuel H. Brown, Joseph D. Walters, Neal A. Sondergaard,
and Howard O. Stevens
Naval Surface Warfare Center

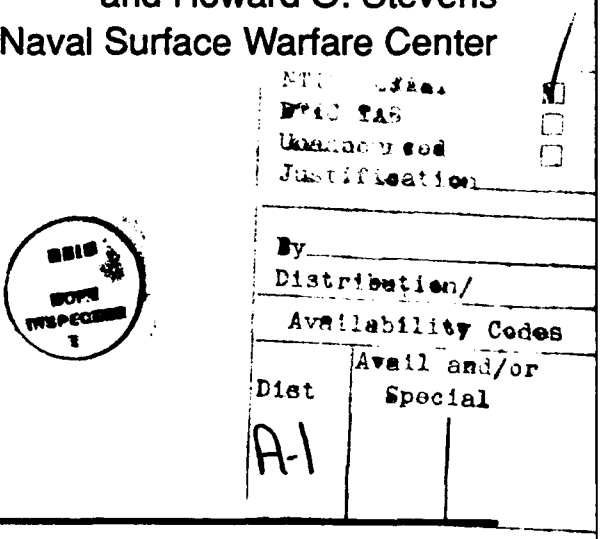

Approved for public release; distribution is unlimited.

CONTENTS

FIGURES

ABSTRACT

A mathematical theory for the performance of a direct current, rectangular duct magnetohydrodynamic (MHD) propulsion system propelling a marine vehicle is presented. The model accounts for the effects of spatially nonuniform magnetic fields and current distributions which are present at the ends of the propulsion unit. The theory is based on an approximate solution of the general MHD duct flow problem in which the mutual interaction of the electric current and fluid flow in a strong magnetic field are considered in detail. For a specified vehicular steady state cruising speed, the propulsive efficiency and electrical power requirements can be calculated from the theory given the hydrodynamic drag of the vehicle and the properties of the fluid medium. Explicit electrical end loss factors are calculated to relate the performance of a propulsor with nonuniform field distributions to the performance of an idealized propulsor with no end losses operating under the same conditions. The power losses due to auxiliary equipment such as electrical generators, buswork, and magnet cryogenic systems are not included in the study.

Numerical results from the models for five design configurations for a nominal geometry under a reasonable range of operating parameters are presented. The numerical results, including the ideal propulsor with no end effects, indicate that the fringing magnetic and current distributions at the ends of the duct generally significantly degrade the propulsive efficiency. The degree of degradation depends on details of the design configuration of the rectangular duct.

ADMINISTRATIVE INFORMATION

This report provides results obtained from a portion of the work on the magnetohydrodynamic (MHD) surface ship assessment studies. This work was completed in FY 91 at the Annapolis Detachment, Carderock Division, Naval Surface Warfare Center (ADCDNSWC) (Code 2712) in conjunction with the Superconductive Propulsion Program at the Annapolis Detachment, Carderock. The work was sponsored by the Office of Naval Technology (ONT–21 James Gagorik). The theoretical studies reported here resulted from a cooperative effort between the Electrical Machinery Technology Branch (Code 2712) of the Propulsion and Auxiliary Systems Department (Code 27) of ADCDNSWC and the Mechanical Engineering Department of the University of Vermont, Burlington, Vermont and the Carnegie Mellon University in Pittsburgh, Pennsylvania.

A condensed version of the work in this report was presented as a paper at the International Symposium on Superconducting Magnetohydrodynamic Ships Propulsion (MHDS 91) at Kobe, Japan, 28–30 Oct.

INTRODUCTION

BACKGROUND

Silent operation of many naval vehicles is crucial to their fundamental mission. It is presently thought that magnetohydrodynamic (MHD) propulsion systems will generate far less acoustic noise than conventional propellor systems though little reliable information on the acoustic signatures of MHD propulsors currently exists.[1] Further, MHD propulsors have no fluid seals or moving parts and so may be more reliable and easier to maintain than conventional systems. Although the efficiencies of MHD systems are known to be significantly less than that of their conventional counterparts, the advantages of MHD propulsors may make their further development for use in marine Navy vehicles attractive. Accurate, detailed theoretical analysis of many aspects of MHD propulsor performance will aid in the continuing development of prototype MHD drive systems.

Recently, Brown et al. published a report describing their mathematical model of a direct-current type MHD propulsor for use in marine vehicles.[1] This report contains the results of an extensive parametric study covering a wide range of operating parameters. In their problem formulation, however, they assume that the spatial distributions of fluid velocity, electrical current, and magnetic field are uniform along the direction of flow. Further, they base their model on velocity and current profiles from a theory that does not account for the interactions among current, velocity, and magnetic field in a detailed way. The present study is made to remove these limitations and so refine and extend the previous analysis in two ways: first, by providing an explicit means to judge the effects of nonuniform fields on a propulsor and, second, by treating the MHD flow problem in a way that accounts for the coupling between the current flow and fluid velocity distributions in a region of strong magnetic field.

In their report, Brown et al. present a model for an idealized propulsor, or one in which there are no end effects. The velocity, electrical current, and applied magnetic distributions are all taken to be uniform along the duct longitudinal axis in this idealized device. Clearly, these distributions must vary somewhat near the ends of a real propulsor of finite length. It will be seen later in this paper that results from performance models of finite length propulsors which consider electrical end effects are significantly different from the corresponding results from models of idealized propulsors which do not consider such end effects. In fact, the assessment of the effects of nonuniformity in the ends on propulsor performance is a main focus of the present analysis.

Moreover, the basis of the model presented by Brown et al. did not fully address effects due to the interaction of electric current flow and fluid flow and so did not accurately represent the physics of the MHD flow problem accurately. The models presented in this paper are based on the asymptotic solution to the MHD duct flow problem in the limit of strong magnetic field and quasi-fully developed flow. The present formulation does account for the interaction between the current and fluid flow in an approximate manner and is more consistent with the true detailed distributions of electric current and fluid velocity at large values of applied magnetic field strength.

OBJECTIVE OF STUDY

The primary purpose of this study is to give a means to obtain numerical estimates of the electrical power losses due to the end effects for an MHD propulsor under known

operating conditions. There are also secondary purposes for this study: first, to give a propulsor performance model which is consistent with the true detailed current and fluid velocity distributions in the MHD flow problem; second, to identify the variables to which the solution is most sensitive in order to aid in system design; third, to show clearly which parameters are fixed by the operating circumstances and which other parameters may be varied at will; fourth, to give optimization methods for adjusting parameters, when possible, to give the best overall performance; fifth, to evaluate some design variations of the propulsor configuration in hopes of improving the efficiency of that device; and, sixth, to identify possible performance problems associated with a generic MHD drive system.

THEORY

GENERAL PROBLEM DESCRIPTION

The generic type of device under study is essentially a direct current electromagnetic pump in which seawater is the electrically conductive working fluid. Of course, the MHD propulsor is limited to marine applications, but it may be adapted to both surface ships and submerged vessels. Seawater enters an inlet nozzle and passes into a straight, constant-area rectangular duct which comprises the MHD drive. Electric current is driven across the duct between a pair of electrodes situated on opposing duct walls. The section of the duct where the electrodes reside is of length L and shall be labelled the center active section. An applied magnetic field is arranged so that it has a large component that is perpendicular to both the current path and the longitudinal axis of the duct. Inside the duct, the fluid experiences a magnetic body force directed down the duct axis given by $\mathbf{J} \times \mathbf{B}$ locally. Seawater is driven through the duct, and the vehicle is propelled forward. A general arrangement diagram of the propulsor is shown in Figure 1, and a schematic diagram of the rectangular MHD drive duct is shown in Figure 2. The propulsor may either be mounted on a pod attached to the vehicle or be built in as an integral part of the vessel. It is assumed throughout the present analysis that the drive is working under steady-state conditions to propel the vehicle along a level, straight-line course in the absence of ocean cross-currents.

SHIP THRUST AND SPEED RELATIONSHIPS

By Newton's third law, the required thrust T under steady operating conditions is equal and opposite to the drag force D on the hull of the vehicle. Given a hull shape, the drag force is uniquely determined by the vehicle speed v_s, which is measured relative to the water far upstream. Therefore, once a design vehicle cruising speed is chosen, the required thrust is known. In many instances, the thrust-speed relation is simple in form. For example, the hull drag for a vehicle travelling so as to have a realistic operating Reynolds number may be expressed simply as: $D = KV^2$. The hull resistance coefficient, K, is approximately a constant for a given fluid and a given hull size and shape. More accurate drag force predictions may be achieved by the use of elaborate drag-velocity relations.

Consider an MHD drive unit as shown in Figure 1. A Cartesian coordinate system will be fixed to the upstream end of the straight-sided section of the drive duct so that the observer moves with the duct. In this frame of reference, all the field quantities are time-steady, assuming constant vehicle cruising speed.

Simple, approximate analytical expressions for both the jet exit velocity and the propulsive efficiency of the MHD drive may be found given a few reasonable assumptions stated below:

- There is no cavitation or starvation of the drive, i.e., the pressure does not fall to zero absolute within the duct.
- The inlet is a well-designed bellmouth such that the friction in the inlet section is negligible and straight duct section always flows full.
- The pod or hull which contains the MHD drive is well streamlined.
- The drive section, which consists of the center active section and the duct extensions, has no changes in cross-sectional area.
- The duct is long and slender so that at the exit the transverse components of linear momentum are very small compared to the component of linear momentum in the direction of the primary flow.
- The fluid is incompressible.
- The thickness of the duct boundary layers are small compared to the duct dimensions, and the velocity profile of the core is nearly flat. These assumptions are consistent with the general nature of magnetohydrodynamic flows. Further discussion of this point may be found later in this paper.

Referring to Figure 1, the steady flow mass continuity equation gives:

$$m = \varrho v_i A_i = \varrho v_d A_d = \varrho v_e A_e = \varrho v_j A_j \quad , \tag{1}$$

where m is the mass flow rate, ϱ is the fluid density, A_d is the local duct cross-sectional area, and v is the local velocity. A jet issues from the exit. At the exit plane, the jet velocity is very nearly equal to the average flow velocity of the duct. Influence on the jet velocity and shape from boundary layers and the transverse momentum effects (e.g., the vena contracta) are very small and shall be neglected; therefore, $v_j = v_e = v_d = \bar{v}$. For a well-streamlined hull or pod, the pressure on the rearward side is approximately equal to the ambient pressure. The pressure inside the jet must match this pressure at the exit (i.e., $P_j = P_e = P_o$.).

The extended Bernoulli equation, which accounts for friction losses, is the total mechanical energy balance for a unit mass of flowing fluid;

$$\frac{v_s^2}{2} = \frac{v_j^2}{2} + w \quad . \tag{2}$$

v_s is the vehicle velocity relative to the water and w is the work done by the fluid per unit mass. The negative of w is simply the work input, per unit mass, to the flowing fluid by the magnetic body force minus the frictional losses at the duct walls on the straight-sided duct section. To reiterate, the friction losses in the inlet bellmouth section are small and are neglected for convenience. Multiplying each term in the extended Bernoulli equation

by the mass flow rate gives a balance of mechanical power in the flowing fluid. The net mechanical work per unit time W done to the flowing fluid is expressed as follows:

$$W = \frac{1}{2}\varrho A_j v_j \left(v_j^2 - v_s^2\right) \quad . \tag{3}$$

Now consider a control volume around the straight duct section as shown in Figure 1. A steady flow linear momentum balance in the z direction gives the following relation for thrust, T, since the flows of momentum in and out of the control volume are equal. The force which propels the ship forward does not come from the acceleration of fluid in the duct, but rather from a reactive force on the magnet coils which impart a magnetic body force on the fluid so that it may move against the adverse pressure gradient on its way through the duct.

$$T = A_d(P_o - P_d) = A_d \Delta P \quad . \tag{4}$$

It is assumed that the inlet bellmouth is so shaped that the pressure over the inlet plane of the straight-sided MHD drive section is uniform. The pressure P_d may then be found by application of the Bernoulli equation.

$$P_d = P_o - \frac{1}{2}\varrho\left(v_j^2 - v_s^2\right) \quad . \tag{5}$$

The exit jet velocity or the average duct flow velocity , $\bar{v}$, in terms of the required thrust, is

$$v_j = \bar{v} = \sqrt{\frac{2T}{\varrho A_d} + v_s^2} \quad . \tag{6}$$

The mechanical power actually expended to drive the ship forward W_s is

$$W_s = T v_s \quad . \tag{7}$$

The propulsive efficiency, η_p, can be expressed as a ratio of velocities:

$$\eta_p = \left|\frac{W_s}{W}\right| = \frac{v_s}{v_j} = \frac{v_s}{\sqrt{\frac{2T}{\varrho A_d} + v_s^2}} \quad . \tag{8}$$

If desired, the thrust may be found in terms of ship speed to give a simplified expression for propulsive efficiency:

$$\eta_p = \frac{1}{\sqrt{1 + \frac{2K}{\varrho A_d}}} \quad , \tag{9}$$

where

$$v_j = v_s \sqrt{1 + \frac{2K}{\varrho A_d}} \tag{10}$$

Examination of equation 10 shows that the jet velocity must be greater than the ship velocity since the hull resistance coefficient, duct area, and fluid density all must be positive quantities. This relationship ensures that the propulsive efficiency is never greater than unity. Physically, the mechanical energy loss in the fluid has a simple interpretation. Some mechanical energy input into the water must be used to accelerate the water up to the jet velocity; the water then jets out from the exit and carries with it some kinetic energy which can not be recovered by the ship. The kinetic energy per unit time discharged from the thruster is $\frac{1}{2}\varrho v_d A_d (v_j - v_s)^2$.

Some further discussion about the friction losses and the design of the inlet and outlet sections of the entire duct is warranted:

- Completely omitting the bellmouth inlet would reduce the propulsive efficiency. For example, a sharp-edged, re-entrant pipe travelling through the water would look somewhat like a Borda mouthpiece and would probably not allow the straight-sided duct section to flow full. The net flow rate for a duct of given area would tend to be low, and poor efficiency would result.

- The use of an exit diffuser section in some duct geometries is probably not warranted. Since the flow would separate from the walls of such a diverging exit section for even modest area expansions, the pressure recovery would be poor. Moreover, a penalty in additional frictional loss would be incurred and the overall propulsive efficiency would be lowered.

- Detailed design of the inlet section and the accounting of the inlet frictional losses is difficult because the flow pattern and the pressure distribution are not known a priori. A full three-dimensional analysis of the inlet flow, including the inertia terms, would be necessary to give the proper inlet shape and to calculate frictional losses. Specification of the inlet shape is not done in the present analysis. Since off-design shapes for the inlet would result in lower efficiencies, the results of this study can be generally taken as best-case estimates of the propulsive efficiency.

- Depending on the design, there may be a spatial pressure distribution on the rearward side of the hull or pod and the jet exit pressure could be somewhat different from the ambient pressure. The resolution of the rearward pressure distribution requires a full three-dimensional flow analysis including the inertia terms.

POWER LOSS MECHANISMS AND EFFICIENCY

EFFICIENCY DEFINITIONS

Power is dissipated in an MHD propulsor system by three major mechanisms: first, Joulean dissipation; second, incomplete transfer of mechanical power from the working fluid to the vehicle; and, third, fluid frictional dissipation. Losses of the first and second type generally dominate the third type of losses under typical operating conditions.

Joulean dissipation always is present in a working propulsor where electrical current is flowing. Generally, of the three loss mechanisms listed above, it is the most important. In real propulsors of finite length, the fringing currents may be large so that the contribution to the total Joulean losses by the end regions may be very significant. Joulean losses are not calculated explicitly in this analysis, although they are represented in all the efficiency calculations as a portion of the total dissipated power.

Incomplete transfer of mechanical power from the fluid to the vehicle occurs because of unavoidable loss of fluid kinetic energy which is transported away by the propulsor exhaust jet. A detailed treatment of this loss mechanism appears in the previous section.

Most fluid frictional dissipation losses are treated in this work, although they are not generally large. An outline of the treatment of this class of losses will be found in later sections of this paper. As with the Joulean losses, they are not calculated explicitly.

There are other losses in the total MHD drive system which have not been accounted for in the analysis. These additional losses could include, but are not confined to, the following: the power input to cryogenic and refrigeration equipment required to maintain superconducting magnets at temperature, losses within the electrical generating equipment attributable to making the electrical power to operate the MHD drive, and conduction losses in the electrical busses which connect the various elements of the system. None of these losses is included in the calculations in the present work.

The overall propulsion system efficiency of the MHD duct or drive efficiency η is defined as the ratio of mechanical power used to propel the vehicle to the electrical power which flows into the device through the duct terminals.

$$\eta = \text{Drive Efficiency} = \frac{\text{Propulsive Power}}{\text{Input Electrical Power}} \tag{11.1}$$

Drive efficiency may also be expressed as the product of the duct efficiency and the propulsive efficiency,

$$\eta = \eta_D \eta_p \tag{11.2}$$

which are defined as:

η_D = Duct Efficiency

$$= \frac{\text{Output Fluid Power of MHD Drive}}{\text{Input Electrical Power}} = \frac{\Delta P \bar{v} A_d}{IV_o} \quad , \tag{11.3}$$

where ΔP is the pressure rise across the duct, $\bar{v}$ is the mean fluid velocity in the duct, A_d is the duct cross-sectional area, I is the total current input to the propulsor duct, and V_o is the applied terminal voltage difference across the duct. Also,

η_p = Propulsive Efficiency

$$= \frac{\text{Propulsive Power}}{\text{Output Fluid Power of MHD Drive}} = \frac{TV_s}{\Delta P \bar{v} A_d} \quad , \tag{11.4}$$

where T is the thrust of the vehicle, V_s is the vehicle speed. These efficiency expressions are further developed in later sections.

Another valuable index of performance, called the end loss factor, is developed which relates the performance of a real propulsor with end losses to an ideal propulsor with no such end losses. Consider a vehicle of a specified design travelling at a known speed. Steady operation of this vehicle then requires an expenditure of mechanical power by the propulsor which is unique to the operating circumstances and is calculable. One can imagine driving this vehicle through the sea at a specified speed, first with a real propulsor and then with an idealized one of identical geometry. Clearly, the ultimate propulsive power output of the two devices must be identical. Therefore, the drive efficiency of either device is directly related to its electrical power consumption. This fact suggests that a good measure of the real propulsor's performance relative to the ideal case with no end losses could be based on the ratio of the required electrical power inputs. Mathematically, this is expressed as:

$$\text{ELF} = \text{End Loss Factor} = \frac{\text{Electrical Power Input to Ideal Device}}{\text{Electrical Power Input to Real Device}} \quad . \tag{12}$$

If the end loss factor (ELF) were known, one could multiply either the duct or drive efficiencies for the idealized propulsor by the end loss factor to obtain the corresponding efficiencies for the real propulsor with end losses.

TECHNIQUES TO LESSEN THE DEGRADATION OF EFFICIENCY DUE TO END EFFECTS

As mentioned before, the drive efficiency for a finite-length MHD propulsor exhibiting significant end effects may be far below the efficiency of an idealized propulsor in which all end effects are neglected. This degradation of efficiency is due primarily to Joulean dissipation associated with fringing currents outside the duct active region. Physical arguments suggest that efficiency degradation may be limited to some degree by appro-

priate modification of either the duct geometry or the structure of the applied magnetic field in the end regions or a combination of the two.

One technique of limiting the efficiency degradation by end effects is the addition of duct extensions of various lengths to the active portion of the MHD duct on both the upstream and downstream ends. It is assumed in the present analysis that the duct extensions are electrically insulating and are of the same cross-sectional geometry as the duct in the active center section. Further, the lengths of the upstream and downstream extensions are assumed to be identical. A schematic diagram of the active center section with its extensions is shown in Figure 3. The physical rationale for the effectiveness of the extensions is as follows. The addition of duct extensions confines the fringing currents to a smaller flow area than they would occupy had those extensions been absent. Confinement of fringing current by duct extensions should then drive the overall resistance to current flow higher and make the Joulean dissipation rate lower.

Another and very important technique of limiting the efficiency degradation due to end effects is to provide a shaped magnetic field structure in the end regions. Magnetic fields outside the active section may interact with the fringing currents in the end regions to provide some pumping which augments the pumping done in the active section. In the present work, the structure of the magnetic field in the end regions may be described by:

$$B = B_o e^{-\xi z} \quad , \tag{13}$$

where ξ is an arbitrary spatial decay constant, B_o is the strength of the uniform magnetic field in the active zone (its maximal value), and z is the location of the station at which the strength of the magnetic field is to be specified, as measured from the end of the active section. Note that z is always taken as positive. A typical field structure of this type is shown in Figure 3. Use of the exponentially graded magnetic field assumption makes the governing equations tractable and provides a means to obtain simple analytical expressions for overall propulsor duct performance. Outlines of the derivation of these performance expressions will be given in later sections. The exponential field decay assumption is justified, since, not only does it allow a wide range of field structures to be examined, but also it gives a rather accurate approximation to the true field structure surrounding an abruptly terminated magnet pole-piece.[2]

Simple physical arguments reveal that the efficiency of the propulsor duct is sensitive to variation in the magnetic field spatial decay constant, and a value for the decay constant may be found that will maximize the efficiency. Consider a propulsor duct with very long insulating extensions operating under conditions where the magnetic field goes to zero abruptly at the ends of the active center section. In this instance, current fringing between the electrodes along any path is driven by the full applied duct terminal voltage difference and no pumping is performed in the end regions. The ends of the active section appear to be electrically shorted and the duct efficiency is rather poor. Now consider a propulsor of identical geometry to the first in which a graded magnetic field is applied to the end regions near the center section. In this case, current fringing between the electrodes along any path is not driven by the full duct termina[illegible]ltage difference but rather by the terminal voltage reduced by an effective back electr[illegible]ve force which is generated along that entire current path. The net fringing current in this instance tends to be less than what it was in the abruptly terminated field case; further, the fringing current

now does some pumping. Moderately extending a graded magnetic field into the end regions thus improves duct efficiency. Finally, consider a propulsor of identical geometry to the first two, where the applied magnetic field is graded in such a way that it extends very far out from the center section into the extreme end regions where the fringing currents have virtually died away to zero. Pumping is still done in the end regions near the active center section, but in the extreme end regions a back electromotive force due to $\mathbf{v} \times \mathbf{B}$ is produced which drives its own currents through the fluid. The duct in these extreme end regions acts as an electrical generator which extracts mechanical energy from the moving fluid by lowering its pressure. In this circumstance, further extension of the magnetic field away from from the center lowers the net pumping effect of the duct and thus reduces duct efficiency. Clearly, an optimal graded magnetic field structure must exist between the limits given by the abruptly terminated field and by the extremely extended field. Since the extent of the magnetic field in space is controlled by the spatial decay factor, an optimal value for the decay factor must exist.

The choices of adding duct extensions or shaping the applied magnetic field or both allow for many different basic propulsor configurations. It is of interest to model these configurations since the arguments just presented suggest that gains in efficiency are attainable by appropriate changes in the basic propulsor design. Because the current fringing distributions could be very different from one configuration to the next, it is necessary to develop separate models for each configuration.

FIVE SPECIFIC DUCT CONFIGURATIONS OF INTEREST

A study of the different possible design choices for duct extensions and for magnetic field structures shows that there are four MHD propulsor configurations which are amenable to mathematical analysis. For comparative purposes, an idealized propulsor with no end losses will also be treated, bringing the total number of cases of interest to five. Other possible propulsor configurations, aside from those above, exist and will be discussed. It will be shown by simple physical reasoning that the nontractable cases have performance bounds that may be approximated by one or another of the results from the four cases that can be analyzed.

Case 1 is the uniform-field, fully developed duct case. The propulsor configuration described by this case is that of a uniform magnetic field which acts over the center active section only. The fluid velocity profiles and the current distributions are, of course, assumed not to change down the duct. Further, all losses due to fringing currents outside the active region are neglected. It should be noted that the case 1 model describes the performance of an idealized propulsor. Results of this case are compared to those of the other cases to explicitly show the dependence of efficiency on end effects. This model gives results for comparison only; it gives valid performance estimates only for propulsors which are so long as to be impractical for use on most sea-going vehicles.

Case 2 is a case in which there are no duct extensions so that current may fringe out into the open sea. The magnetic field distribution of this configuration is uniform over the entire duct, terminating sharply at its ends (Figure 4). In contrast to case 1, the effects of fringing currents outside the center section are treated in detail. These fringing currents do no pumping but give rise to Joulean dissipation. This configuration represents the simplest practical propulsor design. All the cases which follow deal with modifications of this basic design configuration.

Case 3 treats a configuration which is described as a center active section with infinitely long duct extensions with no hydrodynamic surface skin friction. A uniform magnetic field acts over the active center section and terminates abruptly at its ends. This configuration is the simplest modification of the configuration described by case 2. The sole difference between case 2 and case 3 is that in case 3 the currents are confined to an insulating duct, whereas in case 2 they are not. Case 3 is presented, as was case 1, as a basis for comparison for other cases. Since the duct extensions of this case are very long, this configuration is not practical.

Case 4 treats a configuration in which the applied magnetic field consists of a uniform field over the active section and specified exponentially graded magnetic fields over both finite length end regions. The duct extensions over the end regions are taken to be identical, and it is assumed that the local field strength in the end regions is given by equation 13. The duct extensions have magnetohydrodynamic surface skin friction until the exponentially graded magnetic fields are essentially zero. The duct extensions have zero skin friction. Some pumping is done in the end regions in a propulsor of this design configuration, although this pumping is, in general, not done optimally since the extensions are truncated to practical lengths.

Case 5 treats a configuration in which the applied magnetic field consists of a uniform field over the center active section and exponentially graded magnetic fields over the infinite length ends. Again, the duct extensions over the two end regions are taken to be identical, and it is assumed that the local field strength in the end regions is given by equation 13. Again, as in case 4, the magnetohydrodynamic skin friction in the duct extensions is zero when the exponentially graded magnetic field approaches zero. In contrast to case 4, the field in this case is graded to give optimal pumping in the end regions. This case is important since it provides an absolute upper bound on efficiency for any propulsor with a finite-length active section. Furthermore, with the fringing parameter set at the optimal value, the extensions may be truncated to some arbitrary length and the efficiency found by program 4 above. In some situations the actual efficiency predicted by the case 5 program may be approached.

The propulsor configuration described by an active section with finite length extensions and an abruptly terminated field is not treated but is an intermediate case between cases 2 and 3. Clearly the efficiency of this configuration is bounded from below by the efficiency estimate given by case 2 and from above by the efficiency estimate of case 3.

One could arrange a propulsor such that the active section had no duct extensions, but the magnetic field is not sharply terminated at the ends. Some pumping could then occur out in the open sea. Solution of this case would be challenging since the full, coupled set of governing equations for fluid velocity and electric current must be solved in three dimensions by numerical methods. Such a numerical solution would require considerable computer resources making a parametric study of this case prohibitively expensive. Fortunately, cases 2 and 5 provide approximate lower and upper performance bounds, respectively, on this case. Case 2 treats the losses but not the pumping action due to fringing currents in the open sea and so must represent a lower efficiency bound. Conversely, case 5 treats a confined duct with optimal pumping and must represent an upper efficiency bound. It should be noted that these bounds are not exact since the complex interactions of the fluid velocity with magnetic field and electric current in the open sea are not considered in detail. Another closely allied case of possible interest is one of a

propulsor configuration with graded magnetic fields and short duct extensions. In this short extension configuration, some, but not all, of the fringing current may leak out into the open sea. Obviously, this case will also be bounded from below by case 2 and from above by case 5.

BASIC MAGNETOHYDRODYNAMIC FULLY DEVELOPED DUCT FLOW THEORY

GENERAL THEORETICAL CONCEPTS

MHD duct flow is not like ordinary duct flow. The interactions among the applied magnetic field, the electrical current, and the fluid velocity are complex and give rise to unusual distributions of fluid velocity and current not seen in ordinary flows. In this section, solutions to the fully developed MHD duct flow equations for the fluid velocity and electrical current distributions will be discussed for a rectangular duct of constant cross-sectional area. Understanding of the nature of these MHD flow solutions is crucial since they form the basis of all the MHD propulsor models developed in the sections which follow.

One particularly important feature of MHD channel flows is the presence of extremely thin velocity boundary layers, known as Hartmann layers, which are observed on the walls of rectangular ducts in driven MHD flows in an orientation transverse to the direction of the main component of the applied magnetic field. These layers owe their existence to the fact that the velocity of the fluid very near the walls is retarded so that a large back electromotive force in the fluid ($\mathbf{v} \times \mathbf{B}$) cannot be developed there. Electrical current is of higher than average density in the Hartmann layers because the driving electric potential is greater than average. In other words, the Hartmann layers are electrical "shorts" which provide a low resistance conduction path between the electrodes. A significant fraction of the total current carried in the duct travels through the Hartmann layers. Excess electrical current density gives a stronger than average magnetic body force in the Hartmann layers so that the fluid in those layers exhibits very large velocity gradients near the walls. Wall shear stresses along walls with attached Hartmann layers are much higher than those seen in ordinary duct flow situations.

Distinct from the Hartmann layers are secondary layers, so named because they do not exercise primary control over the flow. Secondary layers form along the walls that are aligned parallel to the main component of the applied magnetic field. Velocity and current density distributions within the secondary layers are similar to ordinary duct flow distributions since very little back electromotive force is generated in the direction along the magnetic field lines.

Hunt[3] has reduced the full set of governing equations for general MHD flow (which consist of the Navier-Stokes equations, the continuity equation, Maxwell's equations, and the appropriate constituative relations) to a simplified set of governing equations for fully developed laminar MHD duct flow in rectangular ducts of constant cross-section. Further, Hunt and Stewartson[4] have employed asymptotic expansions of Hunt's governing equations in the limit of strong magnetic field to give simple analytical expressions which approximate the exact laminar, fully developed duct solutions for the velocity and current density distributions. The expressions are written in terms of a dimensionless magnetic

induction, M, known as the Hartmann number. They are valid when the Hartmann number is large (i.e., $M \gg 1$).

The Hartmann number is defined as $M = aB\sqrt{\sigma/\mu}$). B is the applied magnetic induction, σ is the electrical conductivity of the fluid, μ is the viscosity, and $2a$ is the duct width. This parameter may be interpreted physically as the ratio of the magnetic body force to the viscous force. Further, the total magnetic field in the duct is the sum of an applied field generated by currents outside the duct which are completely known, and an induced field generated by currents within the duct which must be calculated. If the induced field strength is very small compared to the applied field strength, the total field is very nearly equal to the applied external field which can be immediately specified. Hunt and Stewartson[4] assume this condition to hold. In mathematical terms ($Rm = a\bar{v}\sigma\mu_o \ll 1$), where Rm is the ratio of the induced field strength to the applied field strength and is called the magnetic Reynolds number. In the above expression, $\bar{v}$ is the average duct flow velocity and μ_o is the magnetic permeability of the fluid. These conditions on the magnetic Reynolds number and Hartmann number are not very restrictive and are almost always met in practical liquid MHD devices.

Following Hunt and Stewartson, a general physical picture can be made of the flow pattern as the Hartmann number becomes large. Figure 5 shows this pattern which may be broken into four regions: Region I designates the uniform velocity core. Region II designates the secondary boundary layers. Region III designates the Hartmann layers. Region IV designates the corner regions. In the limit of a large Hartmann number, the secondary layers have a thickness of order $O(M^{-1/2})$ and the Hartmann layers a thickness of order $O(M^{-1})$ where M is the Hartmann number. The corner regions are usually quite small and will be neglected. Retaining terms of order $O(M^{-1/2})$ or greater in the asymptotic expansions gives expressions which will yield good approximations for the distributions of current density and velocity. These, in turn are manipulated to give relationships among the total current flow, total volumetric fluid flow, pressure gradient, and applied electric potential which form the basis of the propulsor performance models in this work. Frictional pressure losses are embedded in these expressions which are consistent with the structure of the thin Hartmann layers.

It must be emphasized that the MHD flow relationships of Hunt and Stewartson are for laminar flow, and that laminar flow is assumed throughout the present work. This assumption does not introduce serious errors because MHD flows tend to be laminar even at a relatively high Reynolds number if the applied magnetic field is strong. Further, even in turbulent flow, the thickness and structure of the flow-controlling Hartmann layers are in general quite similar to those in laminar flow. Subsequent unpublished numerical analysis of the exact governing equations has been carried out by the authors. These numerical studies indicate that the laminar and turbulent flow models give very similar results for identical operating parameters.

DEVELOPMENT OF THE FULLY DEVELOPED MHD DUCT THEORY

From the basic flow relationships of Hunt and Stewartson, simple approximate equations for dimensionless pressure rise and dimensionless total current may be written for a fully developed duct which is effectively infinite in length, i.e., one that exhibits no

end effects. These equations are quite accurate in most practical liquid MHD flow situations where the Hartmann number is very large compared to unity and the magnetic Reynolds number is very small compared to unity. In terms of dimensionless voltage V^* and the Hartmann number M_o, the dimensionless pressure rise ΔP^* and current I^* are, respectively:

$$\Delta P^* = M_o^2 \left(V^* - 1 - \frac{1}{M_o} \right) \quad ; \tag{14.1}$$

$$I^* = 2M_o(V^* - 1) \quad , \tag{14.2}$$

where the dimensionless quantities are defined as:

$$V^* = \frac{V_o}{2b\bar{v}B_o} \quad , \tag{14.3}$$

$$M_o = aB_o \sqrt{\frac{\overline{\sigma}}{\mu}} \quad , \tag{14.4}$$

$$I^* = \frac{I}{L\bar{v}\sqrt{\sigma\mu}} \quad , \tag{14.5}$$

and

$$\Delta P = \frac{a^2 \Delta P}{L\mu\bar{v}} \quad , \tag{14.6}$$

where $2b$ is the channel depth between electrodes.

The dimensionless voltage V^* may be physically interpreted as the ratio of the applied duct terminal voltage V_o to the back electromotive force developed in the duct from $\mathbf{v} \times \mathbf{B}$. The quantity B_o in the Hartmann number is the strength of the component of the magnetic induction which gives rise to the body force in the fluid (defined as the y component in the present work). In this idealized uniform-field case, it is assumed that B_y is the only component of the magnetic induction present and is uniform throughout the active zone.

The uniform-field, fully developed duct efficiency may be found from the dimensionless pressure rise and current by a nondimensionalizing equation 11.3:

$$\eta_D = \frac{2\Delta P^*}{M_o I^* V^*} = \frac{V^* - 1 - \frac{1}{M_o}}{V^*(V^* - 1)} \quad . \tag{15}$$

These equations form the basis of the performance model for an idealized propulsor configuration previously described as case 1.

Details of the derivation of the above model equations from the asymptotic solutions of Hunt and Stewartson may be found in Hughes and McNab.[5] In addition to application to the fully developed duct flow problem with no end effects, the above relations are also directly applicable to the flow in the active center section, where it is assumed that current density and magnetic field are uniform in all the propulsor configuration models considered in the present work.

PROPULSIVE END EFFECTS CONFIGURATION MODELS

APPROXIMATE THEORY FOR AN MHD DUCT WITH NO EXTENSIONS AND AN ABRUPTLY TERMINATED MAGNETIC FIELD WHICH ALLOWS CURRENT FRINGING

Consider the case where the magnetic field terminates abruptly at the ends of the propulsor duct but where current may fringe out into the open sea. The electrodes are taken to span the entire duct so that its whole length is active. The lack of constraining walls makes this problem difficult mathematically. For an exact solution, the full set of MHD flow equations for the duct interior and the Laplace equation in three dimensions describing electric potential for the duct exterior must be solved together and matched at the duct inlet and outlet. Since the exact governing equations for the duct interior are nonlinear, a numerical solution technique must be used. To treat both the coupled equations in the duct and in the infinite three-dimensional domain outside, numerical solution would consume a great deal of time on a fast computer and make parametric studies very costly. This approach is not adopted in the present work. Instead, a simple analytical approximation of reasonable accuracy based on the Green's function technique is used. Use of this approximate solution for this configuration is justified since it gives a reasonable lower efficiency bound on a specific propulsor design without duct extensions.

Some simplifying assumptions must be made in order to develop the descriptive performance equations for this duct design configuration. The Hartmann number in the duct is taken to be much greater than unity (i.e., $M_o \gg 1$). This condition ensures that the asymptotic solutions of Hunt and Stewartson for velocity and current density distribution are accurate in the duct. This condition is usually met in practice. The magnetic Reynolds number is taken to be much smaller than unity (i.e., $R_m \ll$. This condition allows the induced magnetic field generated by the currents in the duct to be neglected so the the total magnetic field is very nearly equal to the known externally applied magnetic field. This condition is also usually met in practice. The electrode conductivity is assumed infinite so that the whole electrode is at the same potential. In actual practice, the electrode conductivity is very much higher than the fluid conductivity and so may be considered effectively infinite. The total current which crosses the duct inlet or outlet planes outside of the duct openings is assumed to be negligible. The entire duct flow is taken to be fully developed with distributions of current density and velocity which are uniform down the duct axis. This allows the pressure rise across the duct and the current flow within the duct to be given by equations 14.1 and 14.2, respectively. The electric potential distribution at the ends of the duct is assumed to be linear between the electrodes and

constant between the magnet pole-pieces. This assumption is consistent with the notion that the entire duct flow exhibits uniform distributions down the duct axis and that the flow is fully developed. At the ends of the duct, some variation in the profiles of velocity and current density will be seen, but in the light of the other assumptions in this analysis the errors introduced by this assumption are assumed to be tolerable.

The performance model of this configuration is constructed with the aid of the assumptions above. The abruptly terminated magnetic field configuration should give a reasonable lower efficiency bound since it accounts for the Joulean loss but not the pumping effect of the fringing currents in the end regions. In this way, the total pressure rise of the propulsor is given by the pressure rise in the duct alone, while the total current input to the propulsor is the sum of the current input to the duct itself and the current input to the end fringing regions.

In the region exterior to the duct, the flow of current is governed by Ohm's law:

$$\mathbf{J} = \sigma\mathbf{E} = -\sigma\nabla\phi \quad , \tag{16}$$

where $\mathbf{E}$ is the electric field and ϕ is the electric potential. The above equation is true regardless of the fluid velocity since the magnetic field strength is essentially zero there. Treating only the exterior region, it may be deduced from the conservation of electric charge that the governing equation for electric potential is Laplace's equation:

$$\nabla\cdot\mathbf{J} = -\sigma\nabla^2\phi = 0 \quad , \tag{17}$$

except on the duct inlet and outlet boundaries, by writing J in terms of potential as in Ohm's law above. On the duct boundaries there are current sources which emanate from inside the duct. Imagine now two truncating planes which are coincident with the duct inlet and outlet planes as in Figure 4. Ignoring that fraction of the fringing current which crosses the truncating planes outside the duct openings, the true fringing current distribution may be replaced by a current distribution residing in an infinite half-space whose sources lie in a rectangle within the bounding plane of that half-space. Solution of this approximate current distribution by consideration of the electric potential is possible by use of the appropriate Green's function.

Only currents flowing into the half-space are of interest so that current is emitted only over 2π steradians of solid angle about the source point. The Green's function solution for the electric potential on the source plane may then be written in terms of the axial component of current density J_z which crosses the source rectangles:

$$\phi(x,y) = \frac{1}{2\pi\sigma}\int_{y'}\int_{x'}\frac{J_{(z)}(x',y')dx'dy'}{\sqrt{(x-x')^2+(y-y')^2}} \quad , \tag{18}$$

where the primed coordinates indicate the location of a current source point, while the unprimed coordinates indicate the location of a test point. The distributions of electric potential on the duct inlet and exit planes are known from the interior solution, but the current density distribution is unknown. Thus, the given mathematical problem is cast into the form of an integral equation.

For convenience, equation 18 may be nondimensionalized in a way consistent with the nondimensional quantities displayed previously:

$$\phi^*(x^*, y^*) = \frac{1}{8\pi M_o} \int_{y'^*} \int_{x'^*} \frac{J^*_{(z)}\ (x'^*, y'^*)\, dx'^*\ dy'^*}{\sqrt{\alpha^2 (x^* - x'^*)^2 + (y^* - y'^*)^2}} \quad , \tag{19}$$

where,

$$\alpha = \frac{b}{a}$$

which is the cross-sectional aspect ratio, and where

$$J^*_{(z)} = \frac{2aJ_{(z)}}{\bar{v}\sqrt{\sigma\mu}} \quad ,$$

which is the nondimensional current density in the axial direction. The coordinates x^* and y^* are nondimensional coordinates, $\left(\text{i.e.}, x^* = \frac{x}{b},\ \ y^* = \frac{y}{a}\right)$.

Because of the difficulty in solving the exact MHD flow equations in the interior and because of the loss of accuracy incurred by using the half-space equivalent to the true current flow distribution, exact solution of the governing equations is unwarranted. In this analysis, a specific distribution of electric potential at the inlet or exit plane is impressed upon equation 19 which is then solved for the current density distribution. By a previous assumption, the nondimensional electric potential at source rectangle (actually the duct opening on either end) is:

$$\phi^* = -\frac{1}{2} V^* x^* \quad . \tag{20}$$

Electric potential along the y axis must be zero due to symmetry considerations. Once equation 19 is solved, the net flow of fringing current for both ends is computed by integrating the current density distribution over the duct end areas. The power dissipated by current fringing is then taken to be the product of the total fringing current and the voltage difference between the duct terminals and is charged against the duct efficiency.

Although the calculation of the exterior current distribution is now complete and well-posed, it cannot be solved by analytical means. The source plane is broken into discrete cells, and the problem is solved numerically.

Summing the products of current density and area for each cell gives the discrete approximation to the net fringing current leaving the first quadrant. By symmetry, the total current fringing out into the sea is twice that leaving the first quadrant. The discrete approximation to the total dimensionless fringing current to the open sea, I^*_{os}, may then be written for one end of the duct as (see Appendix A):

$$I^*_{os}|_{\substack{\text{one}\\ \text{end}}} = -\frac{1}{\lambda}\sum_{i=1}^{m}\sum_{j=1}^{n} J^*_{(z)ij}\Delta x'^*\ \Delta y'^* \quad , \tag{21.1}$$

where

$$J^*_{(z)ij} = \sum_{k=1}^{m}\sum_{l=1}^{n} M_o G^{*-1}_{1ijkl}\ \phi^*_{kl} \quad , \tag{21.2}$$

and the nodal values of ϕ^*_{kl} are specified by equation 20, and the elements of (G^{*-1}_1) are specified in Appendix (A). λ is defined as $\frac{L}{b}$, and Δx^* and Δy^* are the dimensionless length and width of a computational cell.

The power dissipated in the fringing region is the product of the inter-electrode voltage difference and the fringing current as by a previous assumption. In essence, the fringing current is assumed to be superimposed on the current driven through the center section. Power consumption and mechanical energy input to the water by the center active section are calculated as before. The net power consumption is then the sum of the center section and fringing current power consumption terms. The overall duct efficiency is the ratio of fluid mechanical power input to the net power consumption.

The total dimensionless fringing current may be ultimately found in terms of the dimensionless interelectrode applied voltage by equation 21.2. With the dimensionless fringing current and and equations 14.1 and 14.2 for the duct proper, the dimensionless characteristics of the MHD drive duct with fringing to the open sea may be found as:

$$I^*_T = I^*_C + 2I^*_{os}|_{\substack{\text{one}\\ \text{end}}} = 2M_o(V^* - 1) - \frac{2}{\lambda}\sum_{i=1}^{m}\sum_{j=1}^{n} J^*_{(z)ij}\Delta x'^*\ \Delta y'^* \quad ; \tag{22.1}$$

$$\Delta P^*_T = \Delta P^*_C = M_o^2\left(V^* - 1 - \frac{1}{M_o}\right) \quad , \tag{22.2}$$

and, from (11.3):

$$\eta_D = \frac{2\Delta P^*_T}{M_o I^*_T V^*} = \frac{\text{Output Fluid Power of MHD Drive}}{\text{Input Electrical Power}} \quad . \tag{22.3}$$

The resulting model then describes the performance of the duct configuration labelled case 2.

QUASI-TWO-DIMENSIONAL THEORY FOR EXTENDED MHD DUCTS WITH EXPONENTIALLY GRADED MAGNETIC FIELD IN THE END REGIONS

A general propulsor configuration of particular interest is one that can be described as a center active section with duct extensions and exponentially graded applied magnetic

field in the end regions. In this general configuration, the center active section, where the electrodes reside, is subjected to a uniform magnetic field and may be treated by equations 14.1 and 14.2. Electrically insulating duct extensions of the same cross-sectional geometry as the duct in the center active zone are attached to both the upstream and downstream ends of this center active section. The duct extensions may be of arbitrary length; however, the lengths of the upstream and downstream duct extensions are taken to be equal. In the end regions or those regions outside the center active zone the applied magnetic field grades off from the ends of the center active zone according to equation 13. Although the magnetic spatial decay constant in equation 13 is arbitrary, it is assumed that the decay constants for the upstream and downstream magnetic field distributions are identical. The infinite insulating duct extensions are assumed to be frictionless when B becomes essentially zero. The finite insulating duct extensions are terminated when B becomes zero. The theory for idealized uniform-field, fully developed duct propulsor, as outlined earlier in the paper, may be extended to treat the nonuniform field general propulsor configuration just described. This is done by assuming that the current and velocity distributions vary so slowly down the duct axis that the uniform-field, fully developed duct solution may be applied locally at any axial station in the duct. Full details of the derivation of the performance equations for this configuration may be found in Hughes and Alexion[6] and Hughes et al.[7] This general configuration model may be specialized to give some performance models for specific configurations described earlier.

The development of the general nonuniform-field propulsor configuration model requires a number of assumptions to be made. The Hartmann number, based on the center active section magnetic field strength, must satisfy the condition ($M_o \gg 1$), so that Hunt and Stewartson's asymptotic solutions for current and velocity distributions, which form the basis of the fully developed MHD propulsor model, are accurate in the center section. In practice this condition is almost always met. The appropriate Hartmann number for flow at some location in the end regions should not be based on the maximum magnetic field strength as in the center section, but rather be based on the local magnetic field strength. This is because the asymptotic fully developed MHD duct solutions are taken to hold locally where the magnetic field strength is less than maximal value. Of course, the accuracy of the local fully developed MHD duct solutions degrades in the extreme end regions where the magnetic field dies away virtually to zero. The accuracy of the estimates of both the duct hydraulic losses and the contribution to pumping in the extreme end zones must also be degraded. Fortunately, the contribution to the total pumping action by the extreme end regions is small and the hydraulic losses everywhere in the propulsor are dominated by the Joulean dissipation. This means that one should obtain reasonably accurate estimates of performance for the whole propulsor if the Hartmann number criterion $M \gg 1$ is met for the center section only.

The magnetic Reynolds number Rm must satisfy the condition ($Rm \ll 1$) so the total magnetic field within the duct is very nearly equal to the known applied magnetic field. Fortunately, this condition is generally met in these types of problems. Profiles of current and velocity in the end regions are assumed to change so slowly down the duct axis that they may be considered to be fully developed at any axial location, and the fully developed, uniform-field duct flow solutions may be used locally. This is known as the quasi-fully developed duct assumption. Although this assumption is physically reasonable over most of the the duct, it is unclear whether or not it is valid near the ends of the

electrodes where there could be large axial derivatives of any of the vector components of current density. Both finite difference and finite element studies of the exact MHD duct flow development in two dimensions suggest that even near the ends of the electrodes components of current density show no large axial derivatives. Details of the findings of these two-dimensional studies may be found in Hughes.[8]

The electrodes are taken to have infinite conductivity and so show no variation in electric potential over their surfaces. In practice, the conductivity of the electrodes is generally very much greater than that of the liquid so that the electrode conductivity is indeed effectively infinite. It is assumed that locations far upstream and downstream from the center active section may be chosen where the electric potential is effectively zero.

It is also assumed that magnetic field has only one component which gives rise to a body force in the fluid (defined as the y component in the present work). It is further assumed that the strength of this magnetic field component is taken to be uniform across the span of the propulsor duct at any axial location. The assumptions above must be carefully examined since they cannot be strictly realized in practice, as shown by the following physical argument. The magnetic Reynolds number is small so that the induced magnetic field is small; therefore, Laplace's equation is satisfied by the magnetic field:

$$\nabla^2 \mathbf{B} = 0 \quad , \tag{23.1}$$

which may also be written in terms of vector components in a Cartesian coordinate system as:

$$\nabla^2 \mathbf{B}_x = 0 \ , \nabla^2 \mathbf{B}_y = 0 \ , \nabla^2 \mathbf{B}_z = 0 \ . \tag{23.2}$$

Now consider the major vector component of the magnetic induction **B** in the exponentially graded region. The second axial derivative of this component must be nonzero outside the center zone so equation 23.2 implies that there must be variations in the major field component $\mathbf{B}_y$ along the transverse directions. Equation 23.2 also may imply the existence of other field components. Since practical magnet pole-pieces in the MHD propulsor must be limited in width, equation 23.2 implies that the magnetic field lines must fringe around the outside edges of the pole pieces. These fringing field lines must close on themselves and, so, are curved. Thus, the field lines cannot be aligned parallel to any one coordinate axis at all locations.

The assumptions that the applied magnetic field have a single vector component and may not vary across the span of the duct are not unreasonable. In the present analysis, the magnetic field structure in the end regions is either taken to terminate sharply or to vary slowly down the duct axis. In the first case, the zone where there are large transverse variations of the major field component is very small, while in the second case the axial variations of the applied field are so gradual that the transverse variations of the major field component themselves are small. Further, it will be assumed that the propulsor magnets are well designed so that the magnetic field components transverse to the major component are small. The applied magnetic field strength at any axial location is taken as its spanwise average for the sake of improved accuracy of the model equations.

The fluid velocity profile is assumed to be slug flow with a quasi-fully developed boundary layer. The problem of finding electric potentials and currents becomes un-

coupled from the fluid dynamics with this assumption and a full two-dimensional calculation of electric potentials and currents may be done. Although this is not an exact approach, it does afford more accuracy than using a lumped-circuit model as was done in the previous quasi-one-dimensional model of Hughes and McNab.[5] The slug-flow assumption should be used with some caution. Drastic changes in the velocity profiles in the end regions have been noted; "M"-shaped velocity profiles may form, and there is actually a possibility of flow reversal in the core. Validation of the slug-flow assumption must rest on comparison with two-dimensional solutions of the full, coupled MHD flow governing equations with the fluid inertia terms included.

Given the assumptions above, the governing equation for electric potential may be developed for the end regions. Combining Ohm's law for a moving medium with the charge conservation law in steady state and the definition for electric potential gives, upon manipulation, an equation for electric potential consistent with current flow in the x–z plane:

$$\frac{\partial}{\partial x}\left[\sigma\left(-\frac{\partial \phi}{\partial x}-vB\right)\right]+\frac{\partial}{\partial z}\left[\sigma\left(-\frac{\partial \phi}{\partial z}\right)\right]=0 \quad . \tag{24}$$

Since slug flow is assumed, the above equation reduces to:

$$\nabla^2\phi=\frac{\partial^2\phi}{\partial x^2}+\frac{\partial^2\phi}{\partial z^2}=0 \quad . \tag{25}$$

The boundary conditions for this equation may be formulated as follows if z is now measured from the end of the electrode. At $z = 0$ (the end of the active section) the potential is assumed to be of the form:

$$\phi(x,0)=-\frac{V_o}{2}\left(\frac{x}{b}\right) \quad . \tag{26}$$

As the value of z becomes large, the potential tends toward zero since the magnetic field and fringing current die away. In the limit as $z \rightarrow \pm \infty$:

$$\phi(x,z)=0 \quad . \tag{27}$$

At $x = 0$ (the duct midplane between the electrodes), the potential must be zero since the potential distribution must be antisymmetric:

$$\phi(0,z)=0 \quad . \tag{28}$$

At $x = b$ (the duct wall), the condition that the normal component of electric field must be continuous through the wall implies:

$$\left.\frac{\partial \phi}{\partial x}\right|_{x=b} = -\bar{v}B \quad . \tag{29}$$

Boundary condition (27) makes the above equation very difficult to solve. Therefore, to expedite the solution of electric potential, the problem domain is made finite. Far from the active section, the fringing current and magnetic field die away virtually to zero. Therefore, an arbitrary finite truncation length l_T, as measured from the end of the active section, will be chosen such that the electric potential at that location may be taken exactly equal to zero with little loss of accuracy. Reformulating boundary condition (27) gives:

$$\phi(x, l_T) = 0. \tag{30}$$

It is expected that increasing l_T will improve the solution for potential. Of course, the truncation length is not directly related to the duct extension length; the two need not be equal. However, the truncation length could be used to give a measure of how much fringing current leaks out the open end of a duct extension of specified length. These equations may be nondimensionalized and solved subject to the boundary conditions for a finite domain to obtain the dimensionless electric potential distribution in the end regions.

From the dimensionless electric potential, the dimensionless fringing current and pressure distribution in the end regions may be found from the local application of the asymptotic duct flow solutions of Hunt and Stewartson. Combining these equations with the equations for dimensionless current and pressure in the active center zone gives a total propulsor performance model. The relationships among the dimensionless pressure rise ΔP^*, total current I^*, and applied voltage V^* are found as:

$$\Delta P_T^* = \Delta P_C^* + 2\Delta P_f^*|_{\substack{\text{one} \\ \text{end}}} \tag{31.1}$$

$$= M_o^2\left[V^* - 1 - \frac{1}{M_o}\right] + \frac{2V^* M_o^2}{\tau} - \frac{2V^* M_o^2}{\gamma\tau^2} - \frac{M_o^2}{\tau} - \frac{2M_o}{\tau}$$

$$- 2M_o^2\lambda \sum_{n=1}^{\infty} C_n^*\left[\operatorname{Sinh}\frac{n\pi}{\lambda\gamma}\right]\left\{\frac{n\pi}{\tau^2 + \left(\frac{n\pi}{\gamma}\right)^2}\right\} \quad ,$$

and

$$I_T^* = I_C^* + 2I_f^*|_{\substack{\text{one} \\ \text{end}}} \tag{31.2}$$

$$= 2M_o(V^* - 1) + 2\gamma M_o V^* - \frac{4M_o}{\tau} - 8\gamma M_o \sum_{\substack{n=1 \\ n \text{ odd}}}^{\infty} C_n^*$$

where

$$C_n^* = \frac{V^* - \left\{ \frac{1}{\left(\frac{\gamma'}{n\pi}\right)^2 + 1} \right\}}{\frac{(n\pi)^2}{2} \text{Cosh}\left(\frac{n\pi}{\lambda\gamma}\right)} \quad . \tag{31.3}$$

and with the dimensionless operating parameters of the truncation length ratio $\gamma = \frac{l_T}{L}$, the dimensionless length aspect ratio $\lambda = \frac{L}{b}$, and the magnetic fringing parameter $\tau = \xi L$, which derives from the nondimensional form of equation 13, $\frac{B}{B_o} = e^{-\tau z^*}$. The duct efficiency may be evaluated from the appropriate known dimensionless quantities by the relation (11.3):

$$\eta_D = \frac{2\Delta P_T^*}{M_o I_T^* V^*} \quad , \tag{32}$$

and the model for the performance of the general propulsor duct configuration with extensions and exponentially graded magnetic field is complete. This model may be used without modification to analyze the specific propulsor configurations labelled case 4 and case 5, discussed previously. The model equations of case 4 may be used to build a practical MHD propulsor whose total length (center plus duct extensions) is a reasonable, finite value. One can arbitrarily impose a condition on the total design length, e.g., the total length cannot exceed twice the center section length. Then, one could specify a magnetic fringing parameter to ensure that all but a small specified fraction of the magnetic field is confined to the duct. In this way, a complete set of operating parameters for case 4 may be chosen. The general extended duct configuration model may also be specialized to treat the configuration in which there are long duct extensions present and the magnetic field is sharply terminated at the ends of the active section. Letting the magnetic fringing parameter become very large in equations 31.2, 31.3, and 32 gives the following duct performance equations.

$$\Delta P_T^* = \Delta P_C^* = 2M_o\left(V^* - 1 - \frac{1}{M_o}\right) \quad , \tag{33.1}$$

$$I_T^* = I_C^* + 2I_f^*\Big|_{\substack{\text{one}\\ \text{end}}} = 2M_o(V^* - 1) + 2\gamma M_o V^* - 8\lambda M_o \sum_{\substack{n=1\\ n\,\text{odd}}}^{\infty} C_n^* \quad , \tag{33.2}$$

where now,

$$C_n^* = \frac{2V^*}{(n\pi)^2 \text{Cosh}\left(\frac{n\pi}{\lambda\gamma}\right)} \quad . \tag{33.3}$$

The duct efficiency that may be found from equation 11.3 is written in dimensionless form.

$$\eta_D = \frac{2\Delta P_T^*}{M_o I_T^* V^*} \quad . \tag{33.4}$$

This specialized model may be used to analyze the configuration described previously as case 3.

EXPERIMENTAL VERIFICATION OF THE MODELS

Some experimental findings for MHD duct flows with duct extensions and magnetic field fringing in the end regions are available in the literature, including those of Alexion and Keeton,[9] Alexion,[10] and Nathenson.[11] These reported experimental data are compared to corresponding theoretical results from the quasi-one-dimensional theory of Hughes and McNab[5] and the quasi-two-dimensional theory of Hughes and Alexion[6] and Hughes et al.[7] There is very good agreement between the theoretical calculations and the experimental data which validates the theoretical methods of this analysis.

Alexion and Keeton built an instrumented MHD pump from a stainless steel duct coated with epoxy resin so as to make it electrically insulating. This duct was one component of a flow loop filled with liquid sodium-potassium eutectic alloy or NaK. A throttle valve could be adjusted to apply a desired pressure drop in the loop to be overcome with a pressure rise in the pump duct. Copper electrodes were fitted into windows cut into the steel duct and cemented in place with epoxy. Fluid pressure and electric potential could be ascertained at various locations within the duct by probes. Gross quantities such as the total current input, interelectrode voltage, net pressure rise, duct efficiency, and volumetric flow rate could also be measured.

The duct geometry and some of the operating parameters were reported. The width $2a$, height $2b$, and length of the electrodes of the duct were reported to be 15.2 cm, 17.8 cm, and 23.6 cm, respectively. The spatial decay constant ξ for the external magnetic induction B_o was equal to 0.1 m^{-1}. The magnetic induction through the duct was approximately 0.3 Tesla. The total current between the electrodes in the duct was 16 kA. The voltage across the electrodes was 1.5 V.

One key experiment was performed on the MHD pump apparatus by maintaining a constant net current input for a number of trials while varying the dimensionless voltage. The volumetric flow rate and the total pressure rise across the pump were measured for

each trial so that the pump efficiency could be calculated. A plot of efficiency as a function of dimensionless voltage was then generated. This plot is reproduced here as Figure 6.

Results form the quasi-one-dimensional and quasi-two-dimensional (labelled as "modified one-dimensional" in Figure 9) are shown along with the experimental data. Note that the efficiency scale is expanded so that the comparison of the theoretical and experimental results is actually quite good. The quasi-one-dimensional theory consistently overpredicts the duct efficiency, while the quasi-two-dimensional theory usually underpredicts the duct efficiency. Thus, the theoretical results generally closely bracketed the experimental findings. In this analysis, the quasi-two-dimensional theory was chosen because it was more accurate over the range of operating parameters used in the reported experiments and because it gives a conservative estimate of the duct performance.

INSULATING VANES TO REDUCE JOULEAN DISSIPATION LOSSES

Theoretically, one could mount a number of insulating vanes inside the duct extensions parallel to the walls to increase the net effective resistance at ends of the active section and so reduce the Joulean dissipation due to the fringing currents. Unfortunately, the length of the vanes would significantly reduce the fringing currents and is so long that this technique is not practical in most propulsor applications. Also the vanes would increase the hydrodynamic drag of the propulsor significantly and thus generally lower its propulsive efficiency.

Although the calculation of the exact problem of the fringing current distribution in an internally vaned duct extension is difficult, a simple, approximate solution gives some insight into why the vanes must be very long. Imagine a duct extension with one central insulating vane dividing it into two halves. Now, current could not fringe along the entire duct length; instead, the fringing current would have to flow to the end of the duct extension, fringe outside the end, and then flow back through the entire length of the duct extension back to an electrode. The resistance of the average conduction path of the situation just described could be found assuming a length for the insulating vane. Taking an effective average driving electrical potential difference and the resistance of the vaned duct extension, the fringing current and its associated Joulean loss may be estimated. From calculations like these, it is estimated that a vaned duct extension must be between 30 and 100 duct diameters to be reasonably effective. Of course, one could add more vanes. Analysis of the multivaned duct extension is difficult because of the number of different possible conduction paths to be considered. However, although the Joulean dissipation will be reduced with an increasing number of vanes, the length of the vanes would probably still be significant. Since significant gains in efficiency may be achieved by fringing the magnetic field in the end region rather than installing long vanes in duct extensions, the use of vanes is not recommended.

DEVELOPMENT OF THE TOTAL MHD PROPULSOR SYSTEM PERFORMANCE MODELS AND THEIR NUMERICAL SOLUTIONS

INTRODUCTION

Thus far, a complete set of model equations has been developed to give duct performance for five different duct configurations. Further, equations describing the propulsive performance characteristics of the jet exhaust have also been developed. Combination of the duct and exhaust jet model equations gives an equation set describing the total MHD propulsor system performance. Although the system of model equations is now complete, some additional manipulation and ordering of those equations is necessary for their solution. In some cases, solution of the model equations will require special numerical methods. Details of the manipulation and numerical solution of the model equations will be presented in this section.

It is known from performance studies made for liquid metal MHD pumps that MHD duct efficiency is extremely dependent upon the dimensionless applied voltage V^*, which physically is the ratio of the applied voltage difference across the duct electrodes to the back electromotive force developed in the moving fluid. In pump design, one does have some freedom in adjusting the applied voltage; however, in the MHD propulsor design problem no such freedom exists. It will be shown that the dimensionless voltage is completely specified except in the case where the magnetic fringing parameter may be varied. Even under the latter circumstance, the sensitivity of the dimensionless voltage to variation in the magnetic fringing parameter is not very large. This means that in all cases the dimensionless voltage is essentially fixed by the operating conditions. The consequences of the dependence of the duct performance on the dimensionless voltage set by the operating conditions will be discussed in general terms in this section. Numerical evidence of the relationship between the efficiency and the dimensionless voltage, as set by operating conditions, may be seen in the figures presented later in this paper.

Finally, a general discussion on design optimization will be given in this section, including the optimization of the duct geometry. In the present work, it is assumed that the propulsor will be optimized subject to a fixed and given duct geometry. Of course, changing the duct geometry does have an effect on propulsor performance and should be considered in the complete optimization of an MHD propulsor design. Numerical cases showing the dependence of duct performance on geometry will not be made in the present analysis, however, some general trends will be discussed in the light of previous work on dc liquid metal MHD pumps in order to expedite any future research made along these lines.

GENERAL SOLUTION PROCEDURE

The estimation of the total system performance for any case requires a logical ordering of the set of model equations. This order is very similar from one specific propulsor configuration to the next. Basically, the solution proceeds as follows:

- Fluid properties for the conditions of interest are established.
- Maximum possible magnetic field strength is chosen.

- A nominal propulsor duct geometry is chosen. This includes the length of the duct electrodes (length of the center active section), the height and width of the duct, and the length of the duct extensions, if any.
- The design vehicle cruising speed and the hydrodynamic resistance coefficient for a given hull shape are established.
- The value of the magnetic fringing parameter will either be set to a practical value or varied to give optimum performance. The value of the fringing parameter may be made very large in which case the magnetic field structure will terminate abruptly at the ends of the center active section.
- The required vehicle thrust is calculated from equation 7.
- The required duct pressure rise to give the necessary thrust is found from equation 4.
- The mean flow velocity of seawater in the duct is found from equation 10.
- Propulsor efficiency is found from equation 9.
- Basic dimensionless parameters describing the flow, such as the Reynolds number, the magnetic Reynolds number, and the Hartmann number, may be computed. Values of these numbers are substituted into the solution accuracy criteria, e.g., $M \gg 1$, so that the possibility of obtaining an accurate final solution can be ascertained.
- Dimensionless pressure rise is computed. Certain aspect ratios for the duct are computed according to the duct configuration chosen.
- Once the Hartmann number, the dimensionless pressure rise, the magnetic fringing parameter, and the duct aspect ratios (if they apply) are known, consideration of the set of descriptive equations for a particular duct configuration will allow the solution of the dimensionless voltage ratio and the dimensionless input current for that case.
- Values for the voltage and current are easily found from their nondimensional counterparts. Total input power is the product of the input current and interelectrode voltage.
- Duct efficiency is calculated from the Hartmann number, the dimensionless pressure rise, the dimensionless input current, and the dimensionless voltage.
- Multiplying the duct and propulsor efficiencies gives the total drive efficiency as in equation 11.2.
- The efficiency of a propulsor with fringing electric currents may be compared to the efficiency of an idealized propulsor with no fringing currents by the end loss factor (ELF) given by equation 12.

Upon completion of the final step, all the performance characteristics are known. All the steps above are straightforward with the exception of determining the dimensionless voltage ratio and the dimensionless input current for each specific case. This is because the duct performance models, as written, relate pressure and total input current to the applied voltage. In the above solution scheme, it is the pressure rise and not the applied voltage, which is specified. Therefore, the equations are inconvenient to solve as they stand. Manipulation of each of the duct performance equations will be discussed in turn in the sections to come.

GENERAL DISCUSSION OF PERFORMANCE, OPTIMIZATION, AND THE PROBLEM CONSTRAINTS

In this section, the general problem of propulsor optimization is addressed. The important effects of dimensionless voltage on duct performance are discussed, as well as some general trends of duct performance with the variation duct geometry.

It has been known from previous studies of dc liquid metal MHD pumps that the duct performance is extremely dependent on the dimensionless applied voltage, see Hughes and McNab.[5] In the design of MHD propulsors, this dimensionless voltage is essentially fixed. Some possible counterintuitive results that could arise from the consequences of this dependence on dimensionless voltage will be discussed.

Consider the duct efficiency for an idealized propulsor with no end losses (case 1) defined by equation 15 shown below for reference.

$$\eta_D = \frac{V^* - 1 - \frac{1}{M_o}}{V^*(V^* - 1)} \quad . \tag{34}$$

One may now study the efficiency of a hypothetical propulsor, given a duct geometry and physical properties of the fluid medium, as a function of V^*, the applied dimensionless voltage ratio. From the above equation, it is evident that upon fixing the value of the Hartmann number M_o, the efficiency is only a function of dimensionless voltage. Note that no constraint has been placed on the duct pressure rise. In fact, the duct pressure rise and, consequently, the net propulsor thrust must vary with the applied duct voltage. The dependence of efficiency on V^* is very strong for typical values of the Hartmann number.

Choosing one such typical Hartmann number as $M_o = 1{,}000$ gives an efficiency curve as shown in Figure 7. Observe that for a value of V^* very close to unity, the efficiency is zero. Beyond the point of zero efficiency, the efficiency rises very rapidly with increasing V^* to reach a peak and then rapidly fall off. The general shape of the curve describing efficiency in terms of dimensionless voltage for case 1, as shown in Figure 7, is taken to be representative of such curves for all the other cases. This is not unreasonable since, not only do the other cases describe configurations in which a significant fraction of the pumping effect comes from the center section where the equations of case 1 apply directly, but also the losses and pumping effects in the end regions are based on the local application of the same profiles of velocity and current density that led to the duct model equations of case 1.

At the point when the appropriate duct performance model is to be solved (the twelfth step in the general solution procedure as outlined in the previous section), the dimensionless pressure rise, the Hartmann number, and various length ratios of the duct are known. In all the duct performance models, there are two equations to be solved for two unknowns, namely: the dimensionless applied voltage and the dimensionless total input current. Note that in the duct model equation sets for cases 1, 2, 3, and 4, the value of the dimensionless applied voltage is completely determined. In case 5, the dimensionless applied voltage in dependent on the magnetic fringing parameter, but this dependence is rather weak. Thus, the applied dimensionless voltage is essentially fixed by the operating parameters and the duct efficiency determined in all the cases considered. Using the previous example of the idealized propulsor (case 1), the value of V^* given by the imposed operating conditions determines an operating point on an efficiency curve such as Figure 7.

From simple physical reasoning, one might expect that the duct efficiency for a given hull design and center section magnetic field strength should monotonically decline with increasing speed; this is not necessarily true. The strong dependence on the dimensionless voltage, which itself is fixed by the operating parameters, significantly influences the efficiency and can actually cause the duct efficiency to rise with increasing vehicle velocity.

A simple, though not generally correct, argument for the dependence of efficiency on vehicle speed is as follows: For a given hull shape, the thrust requirement goes as the square of the vehicle velocity. Body force is derived from $\mathbf{J} \times \mathbf{B}$ integrated over the duct volume. A larger thrust requirement means that an increased magnetic body force over the duct volume is necessary. Maintaining a constant magnetic field strength requires that the net electrical current must be larger as the required thrust increases. The effective electrical resistance of the duct is approximately constant so that the Joulean losses in the duct go as the square of the net current. Joulean losses make up the bulk of the total losses so that efficiency must decline with increasing vehicle speed.

The above argument would be certainly valid if the effective voltage across the duct electrodes, defined as the applied voltage minus the net effective back electromotive force, had a weak dependence on the operating parameters. However, this is not the case. The duct efficiency may be driven rapidly upwards by relatively small changes in V^*, as seen in Figure 7. In some circumstances, the increase in efficiency due to the dimensionless voltage effect dominates and duct efficiency actually increases with vehicle speed.

Examination of the duct performance models for the various configurations shows that the magnetic fringing parameter is the only possible free parameter if the duct geometry is specified since V^* cannot be optimized. Indeed, the fringing parameter in case 5 is optimized. However, in all the other cases even the fringing parameter is fixed so there are no free parameters and optimization is impossible.

Of course, the duct efficiency depends on the duct geometry, so the possibility of optimization of the duct geometry exists. Different schemes, based on adjusting different duct dimensions, are possible. Some of these schemes are discussed below in the light of previous experience with dc MHD pump analyses to expedite some lines of future research.

It is expected that small values of the duct cross-sectional aspect ratio $\alpha = \frac{b}{a}$ would give better efficiency than large values of that parameter since the effective electrical duct resistance in the former circumstance would be lower. This effect was shown in calculations by Hughes and McNab.[5] In practice, the construction of ducts with small values for the cross-sectional aspect ratio generally carries a severe penalty. Because magnetic flux must be driven through the long dimension of the duct cross-section for small α, it is more difficult to generate the necessary magnetic field than in ducts with large α. In the past, conventional magnets were used to drive MHD pumps, which required large amounts of electrical power. The marginal increase in magnet input power required in these systems for a decrease in α outweighed the efficiency gains in the duct. A study of such a system with superconducting magnets replacing the conventional ones would be interesting. Such a study might show that tall, thin duct sections with low values of α may give net efficiency gains over more nearly square duct sections working under the same operating conditions.

One could vary the duct active section length in order to optimize the propulsor. Indeed, the existence of an optimum length was shown in the calculations of Hughes and McNab.[5] Unfortunately, the sensitivity of efficiency with duct length is generally low and the optimal length is impractically large.

Making the duct cross-sectional area large increases both the duct and propulsive efficiencies. A large duct area makes the duct pressure rise for a given required thrust small. One sees the effect on duct area on propulsive efficiency directly from equation 9. Moreover, duct efficiencies should generally increase as duct area increases. For a given duct cross-sectional aspect ratio, fluid properties, and base magnetic field strength, the Hartmann number must increase with increasing duct area. Generally, the higher the Hartmann number, the more efficient the propulsor. This dependence is also noted in the paper of Hughes and McNab.[5]

NUMERICAL METHOD FOR SOLVING THE FULLY DEVELOPED MHD PROPULSOR MODEL WITH NO FRINGING (CASE 1)

This case presents no numerical difficulties. Equation 14.1 may be solved for V^* in terms of ΔP^* and M_0, which are known. Equations 14.2 and 15 then give the dimensionless input current and duct efficiency immediately.

NUMERICAL METHOD FOR SOLVING AN MHD PROPULSOR DUCT WITH NO DUCT EXTENSIONS AND AN ABRUPTLY TERMINATED MAGNETIC FIELD, WHICH ALLOWS CURRENT TO FRINGE INTO THE OPEN SEA (CASE 2)

In this case, a matrix inversion is required to solve the discrete approximation to the governing integral equation for the fringing current. A computational grid is arranged on the current source plane as described previously in the paper, and the axial current density is computed from the geometry and the known distribution of electric potential. Because a discrete approximation to the governing equation is used, the accuracy of the result depends on the fineness of the computational mesh. It is suggested that the mesh be refined in a number of successive trial computations until a grid-independent solution is obtained.

Since there is no pumping outside the center section, the duct pressure rise is solely attributable to the center section. Solving equation 22.2 for V^* immediately gives the value of that parameter. Once the applied dimensionless voltage is known, the electric potential of each grid node is calculated from equation 20.

The nodal electric potentials are related to the nodal axial current densities by an influence coefficient matrix $\underline{G}_1^*$, elements (see Appendix A for details). To solve the current density distribution given the potential distribution, this influence matrix must be inverted. The LU decomposition method was chosen for this purpose because of its speed. The influence matrix is full so that no special methods for sparse matrices would apply. This method is fully described elsewhere.[12]

Upon calculating the inverse of the influence coefficient matrix, the nodal axial current densities may be found. The total input current may then be found directly from equation 22.1. Duct efficiency follows simply from the dimensionless total pressure rise and input current from equation 22.3.

NUMERICAL METHOD FOR THE SOLUTION OF AN MHD PROPULSOR WITH FRICTIONLESS, INFINITE LENGTH EXTENSIONS AND AN ABRUPTLY TERMINATED MAGNETIC FIELD (CASE 3)

Case 3 requires the calculation of an infinite series for the fringing current. An algorithm is used which truncates the infinite series so that the error in the finite-term approximation is in some measure small.

Since $B = 0$ outside the active section, there is no pumping effect in the end regions so that the duct pressure rise is attributable solely to the center active section. Dimensionless voltage V^* may be found by the solution of equation 33.1. Then, the total dimensionless input current may be found by solution of equation 33.2 which contains an infinite series which must be truncated at some point. After the calculation of each new term in the infinite series, the relative change in the partial sum due to the addition of that term is calculated. The series is truncated at the term which gives a relative change in the partial sum less than a predetermined tolerable relative error bound. The duct efficiency is then simply found from the dimensionless total pressure rise and dimensionless total input current by substitution in equation 33.4.

NUMERICAL METHOD FOR THE SOLUTION OF AN MHD PROPULSOR WITH FINITE LENGTH DUCT EXTENSIONS AND A SPECIFIED EXPONENTIALLY DECAYING FRINGING MAGNETIC FIELD (CASE 4)

The duct extensions have magnetohydrodynamic skin friction until the exponentially graded magnetic field is essentially zero. Then the duct friction becomes zero. This case is a generalization of case 3 and, so, also requires the summation of infinite series. These series are computed exactly as described in the previous case. Now, however, there is a pumping effect in the end regions so that the dimensionless voltage cannot be easily calculated from the total dimensionless pressure rise and a special solution method is required.

The solution of this case proceeds as follows. A reasonable initial guess for the dimensionless voltage is made. Dimensionless total pressure rise and dimensionless total input current are found in equations 31.2 and 31.3, respectively. The duct pressure rise

calculated during the present iteration is compared to a target duct pressure rise needed to meet the thrust requirement of the propulsor. A pressure error index is defined as the absolute value of the relative error in the pressure or mathematically:

$$\text{Pressure Error Index} = \left| \frac{P - P_{\text{Target}}}{P_{\text{Target}}} \right| .$$

If the pressure error index is below a preset tolerable error bound, calculation stops; if not, the dimensionless voltage estimate is updated and the cycle repeats beginning at the second step.

The appropriate adjustments on the estimate for dimensionless voltage are made by minimizing the pressure error index by the method of Powell.[12] This method was chosen because of its speed, flexibility, and robustness. However, some modification to the minimization algorithm had to be made. Powell's method does optimization without constraints or, in terms of this work, Powell's method places no bounds on the estimate of V^*. During the course of the solution procedure, V^* may be assigned a physically impossible value and a spurious answer would result. To avoid this problem, a penalty function is added to the pressure error index to yield a new function called the objective function. The penalty function is given the value zero whenever a physically realizable estimate for V^* is chosen and a very large value positive value when the V^* estimate is not physically realizable. By minimizing the objective function rather than the pressure error index alone, a physically realizable solution is assured.

Once iteration has stopped, the total dimensionless current, dimensionless voltage, and the total dimensionless pressure necessary to give the required propulsor thrust are known. Duct efficiency follows immediately from equation 32.

NUMERICAL METHOD FOR THE SOLUTION OF AN MHD PROPULSOR WITH INFINITE LENGTH DUCT EXTENSIONS AND AN OPTIMALLY GRADED EXPONENTIALLY DECAYING FRINGING MAGNETIC FIELD (CASE 5)

The solution procedure for case 5 is nearly identical to that of case 4 and uses the same model equations. The difference between cases 4 and 5 is that in the latter both the dimensionless voltage and magnetic fringing parameter are adjusted at every iteration by Powell's minimization routine. The objective function of this case consists of three terms: a penalty function to ensure that the updated estimates for dimensionless voltage and magnetic fringing parameter are physically realizable, the negative of the duct efficiency, and the pressure error index, as defined in the previous section. By minimizing this objective function, the efficiency is maximized while the necessary condition on duct pressure rise is met. Powell's method works well here and eliminates an iteration loop, allowing rapid calculation of the final solution.

NUMERICAL RESULTS AND DISCUSSION

Calculations have been made using the five duct configuration models discussed previously in the paper. The nominal duct width $2a$ was 4 meters, the height $2b$ was 4 me-

ters, and the length L was 10 meters. The density ϱ, viscosity μ, and conductivity σ of the seawater were taken as 1.03×10^3 kg/m, 1.00×10^{-3}/N–s/m, and 4.00 S/m, respectively.

Two separate sets of calculations were done, the first based on a hull with low drag (K = 1,500), and the second based on a hull with moderate drag (K = 3,000), where, K is the hull hydrodynamic resistance coefficient. A range of vehicle velocities v_s was chosen where 2.50 m/s was the low value and 25.0 m/s was the high value. In each set of calculations, two different center-section magnetic induction values B were taken which represent the lower and upper bounds on a reasonable range of design values. The value of 6.00 Tesla was the lower value, and 10.0 Tesla was the higher value.

In Figures 8 through 13, the numbers 1 through 5, designating different curves, represent cases 1 through 5, respectively, with a 6 Tesla field in the center active section of the MHD duct. The numbers 6 through 10, designating different curves, represent cases 1 through 5, respectively, with a 10 Tesla field in the center active section of the MHD duct.

Consideration of all these parameters completely specified the operating conditions in all cases except case 4. For that case, the total duct length (center plus duct extensions) is taken as 20.0 m or twice the length of the center active section. To ensure that all but a small fraction of the magnetic field is confined in the duct, the magnetic fringing parameter was set as $\tau = 6.0$ (i.e., $\tau = \xi L$), so that at the outside end of the duct extension of length 5.00 m, the magnetic induction B is less than 5% of its center section value. It is assumed that the field outside the duct in the open sea has very little effect on the final result.

Results of the calculations for the low drag hull are displayed in Figures 8 through 10. All the curves presented show dependence with vehicle velocity and center-section magnetic induction. Duct efficiency η_D is presented in Figure 8, drive efficiency η in Figure 9, and the end loss factor (ELF) in Figure 10. Similarly, the results of the calculations for the moderate drag hull are displayed in Figures 11 through 13, again showing dependence with vehicle velocity and magnetic field strength. Duct efficiency is presented in Figure 11, drive efficiency in Figure 12, and end loss factor in Figure 13.

Upon examination of the curves of duct efficiency in Figures 8 and 11, some overall patterns may be discerned. There is, as expected, a general decline in efficiency with increasing speed. However, for certain ranges of the operating parameters the duct efficiency, as calculated by some of the duct configuration models, may actually increase with vehicle speed. This is due to the dimensionless voltage sensitivity effect, where a rather small change in the dimensionless voltage, itself determined by a change in the basic operating parameters, gives a rapid rise in the duct efficiency. This effect was discussed previously in the paper.

Further, it is seen that duct efficiencies are generally higher for increasing magnetic induction B, though there are exceptions to this rule also. The reason that higher magnetic field strength in certain circumstances gives lower efficiency, duct configuration and all other operating parameters held constant, is again due to the dimensionless voltage sensitivity effect. This fact can be seen immediately by examining the dimensionless voltage $\left(V^* = \frac{V_o}{2b\bar{v}B_o} \right)$.

The dependence of the duct efficiency on V^* still comes into play, but now V^* changes with B_o instead of $\bar{v}$. If the operating point on the appropriate duct efficiency vs. dimensionless voltage curve is near the peak, an increase in magnetic field may drive the efficiency down sharply.

More general trends may be seen by comparing the duct efficiencies for all five duct configurations under the same operating conditions. Case 2 consistently gives the lowest efficiencies in the group, typically from 10% to 30%. This is expected since case 2 does not account for any pumping in the open sea but charges all the Joule loss due to the fringing electrical current against the duct efficiency. Case 3 consistently gives a better duct efficiency than case 2, although the difference between the two is only a few percent. This, too, is expected since no pumping in the end regions is done in case 3 and the confinement of the fringing currents in the duct gives a current distribution which is not markedly different from the distribution found in case 2. Case 4 consistently gives a duct efficiency higher than that of case 3. The duct efficiency of case 4 may rise to approximately 50%. This configuration model is especially important since it gives estimates for a propulsor that is actually practical to build, that is to say one of reasonable length. Case 5 gives efficiencies that are consistently higher yet than the corresponding results from case 4 because the magnetic field distribution is optimized. The duct efficiency estimates of case 5 are the highest possible for a propulsor with a finite-length active section where end losses must be considered. The duct efficiencies of case 5 may be as high as 70% or more. Unfortunately, the duct configuration implied by case 5 is impractical since very long duct extensions must be used. Finally, the ideal propulsor model of case 1 gives the highest duct efficiency of all the configurations for low vehicle speeds, but surprisingly its efficiency is surpassed by case 5 at high speeds. This counterintuitive result again stems from the dimensionless voltage sensitivity effect. The duct efficiency is never more than a few percent over that of case 1 so that the results of case 1 may be taken as an approximate upper limit on propulsor efficiency for the configurations studied.

The total drive efficiency curves of Figures 9 and 12 are very similar to their duct efficiency counterparts and have the same basic shapes. Of course, the degradation of drive efficiency with speed is more severe than that of duct efficiency as seen from the formula for the propulsive efficiency given as equation 9.

The end loss factor curves of Figure 10 and 13 show that the spread in the efficiencies of the five different duct configuration models decreases with increasing speed. Extension of the speed range studied is necessary to determine whether or not this trend continues at higher vehicle speeds.

Figure 14 shows the dependence of duct efficiency on the magnetic fringing parameter, holding all other conditions constant, for the nominal case where: $L = 10.0$ m, $2a = 4.0$ m, $2b = 4.0$ m, $K = 3{,}000$.

Note that the curve shows the existence of an optimal magnetic fringing parameter. For values of the fringing parameter of about unity or less, the curve shows that the sensitivity of duct efficiency on magnetic fringing parameter is very slight. Of course, as the magnetic fringing parameters are made smaller, the extent of the field structure is increased.

SUMMARY AND CONCLUSIONS

A mathematical theory for the performance of a direct current electromagnetic seawater pump for the propulsion of marine vehicles was developed that accounts for the effects of spatially nonuniform distributions of electric current and applied magnetic field. Power losses both due to the loss of kinetic energy by the vehicle exhaust jet and by hydraulic friction and Joulean dissipation in the propulsor duct were carefully considered. Analysis of the duct performance was based on asymptotic solutions to the full, coupled MHD flow problem for current and fluid velocity distributions in the duct. These solutions are generally valid for typical design operating conditions.

Three main simplifying assumptions have been made in the present work:

1. The flow at any axial location in the duct is fully developed locally.

2. The MHD flow profiles for fluid velocity and electric current are given locally by the high Hartmann number duct flow solutions of Hunt and Stewartson.[4] Fluid turbulence does not significantly affect the velocity profiles or the overall performance of the MHD propulsor.

3. The magnetic induction field structure in the end regions is approximated by an exponentially decaying field.

The general validity of these assumptions has been substantiated by the authors by subsequent numerical analysis of the exact two-dimensional governing equations for both laminar and turbulent flows. Results of these numerical studies will be made available in a forthcoming published report.

Different means of improving propulsor system efficiency were discussed with emphasis on adding electrically insulating duct extensions to the center active section of the duct and on grading the magnetic field in the end regions. Consideration of these design options necessitated the development of five different MHD propulsor models for each of the following duct configurations. Case 1 modelled a uniform-field, fully developed duct propulsor with no end effects. Case 2 modelled a duct with no duct extensions and an abruptly terminated magnetic field which allowed current to fringe out into the open ocean. Case 3 modelled a frictionless duct with infinite length extensions and an abruptly terminated magnetic field. Case 4 modelled a duct with finite length extensions and a specified exponential grading of the magnetic field in the end regions. Case 5 modelled a duct with infinite length extensions and an optimally graded exponentially decaying magnetic field in the end regions. In cases 4 and 5, the duct extensions had magnetohydrodynamic skin friction until the magnetic field decreased to essentially zero. Specific model equations were developed for each of these cases, and the appropriate numerical methods for the solution to those model equations were given.

It was shown that, for a given duct geometry, the models described as case 1 through case 4 had no free parameters and so could not be optimized. The magnetic fringing parameter was identified as the only free parameter for case 5. Further, it was shown that the dimensionless voltage is essentially fixed for given operating conditions for all five models. The strong dependence of the duct efficiency on dimensionless voltage was illustrated by some manipulation of the idealized propulsor model with no end effects (case 1). The extreme sensitivity of duct efficiency with dimensionless voltage was shown to give strange and counterintuitive results over some ranges of operating parameters.

Computer programs were generated to solve each of the five duct configuration models. These programs were used to produce efficiency curves for a nominal propulsor geometry for different values of applied magnetic field and vehicle velocity. An end loss factor was defined which compares the performance of a propulsor with end effects to an idealized propulsor with no such end effects. End loss factors for all the numerical runs were made.

According to the mathematical models developed in this paper, some conclusions may be drawn by comparing results from the numerical computations performed so far. It appears that the proper fringing of the magnetic field in the end regions is the single-most important means of obtaining good duct efficiencies. The idealized propulsor with no end losses gives an approximate upper bound on the performance of the duct. This efficiency may be slightly exceeded, however, by the imposition of a near-optimal magnetic field structure on the end regions of the propulsor. Case 4 is the most important case from a practical standpoint since it allows for a propulsor of finite length. For typical applications, it appears that the magnetic fringing parameter is far from its optimal value. Use of a near-optimal magnetic fringing parameter would give a duct design with extensions that are so long as to be impractical. This means that a practical MHD propulsor system design would, in general, have an overall drive efficiency a good deal less than an idealized propulsor with no end losses running at the same operating conditions. The MHD propulsive efficiency results presented in this paper can only be considered valid for rectangular ducts with the configurations modelled, but may yield insights into others.

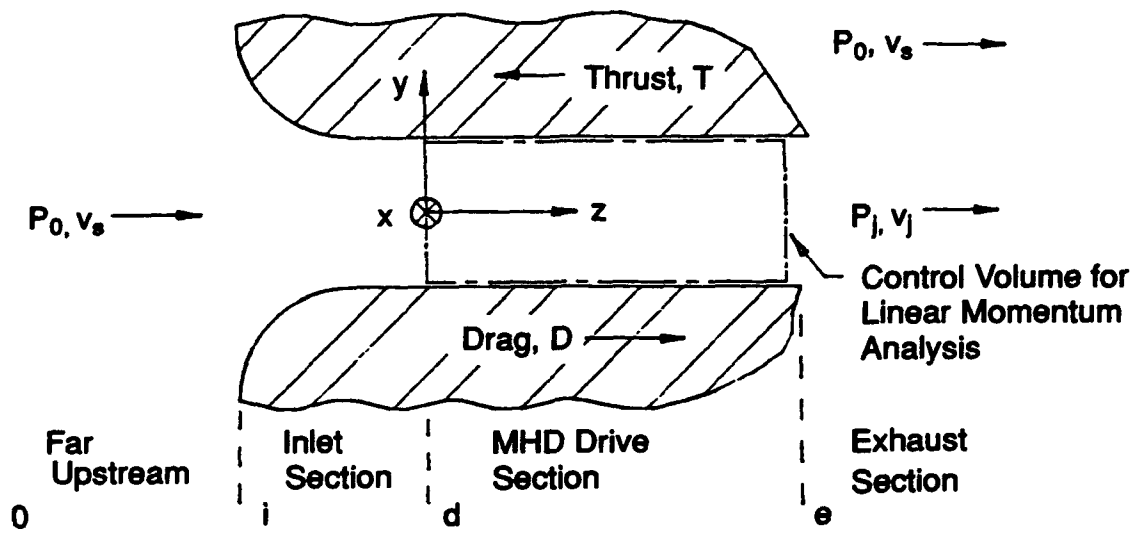

Figure 1. General arrangement diagram of a direct current MHD vehicle propulsor, showing fluid pressure and velocity at various stations. (Drive housing diagram is meant be be generic; no specific design details are implied.)

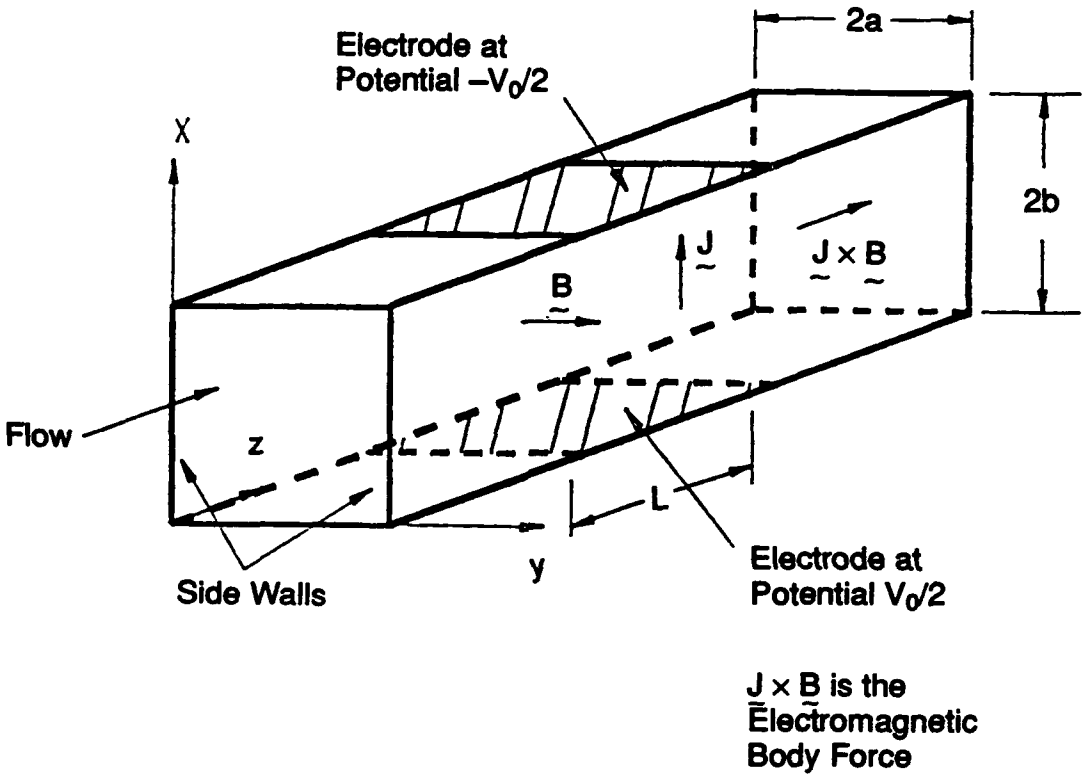

Figure 2. The geometry of the MHD propulsor drive duct (as seen from the top.)

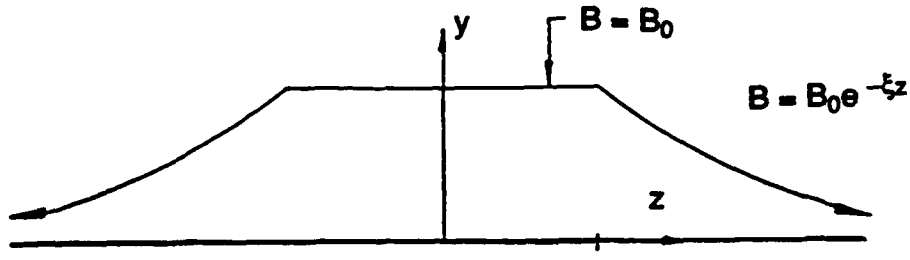

Magnetic Field Structure

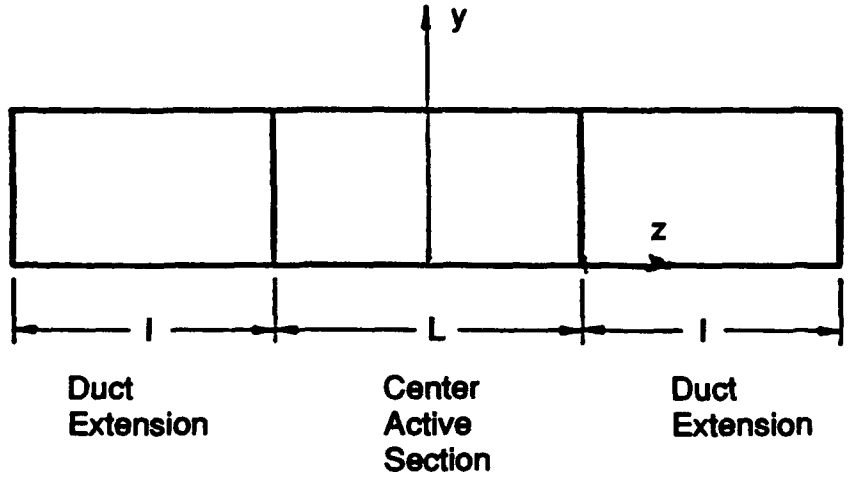

Duct Geometry

Figure 3. General diagram of the MHD propulsor duct showing the duct extensions and structure of the exponentially graded magnetic field.

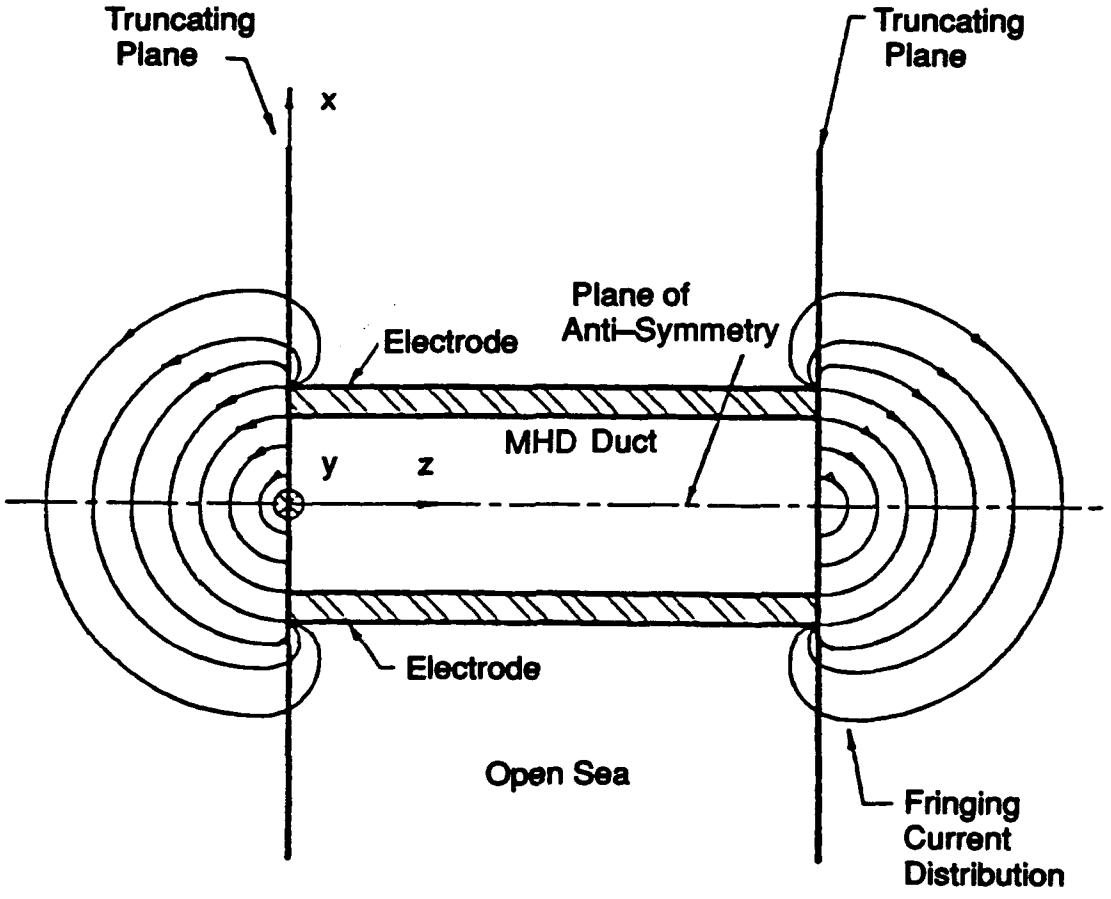

Figure 4. Cross-section of MHD propulsor through the mid-plane with current fringing into the open sea.

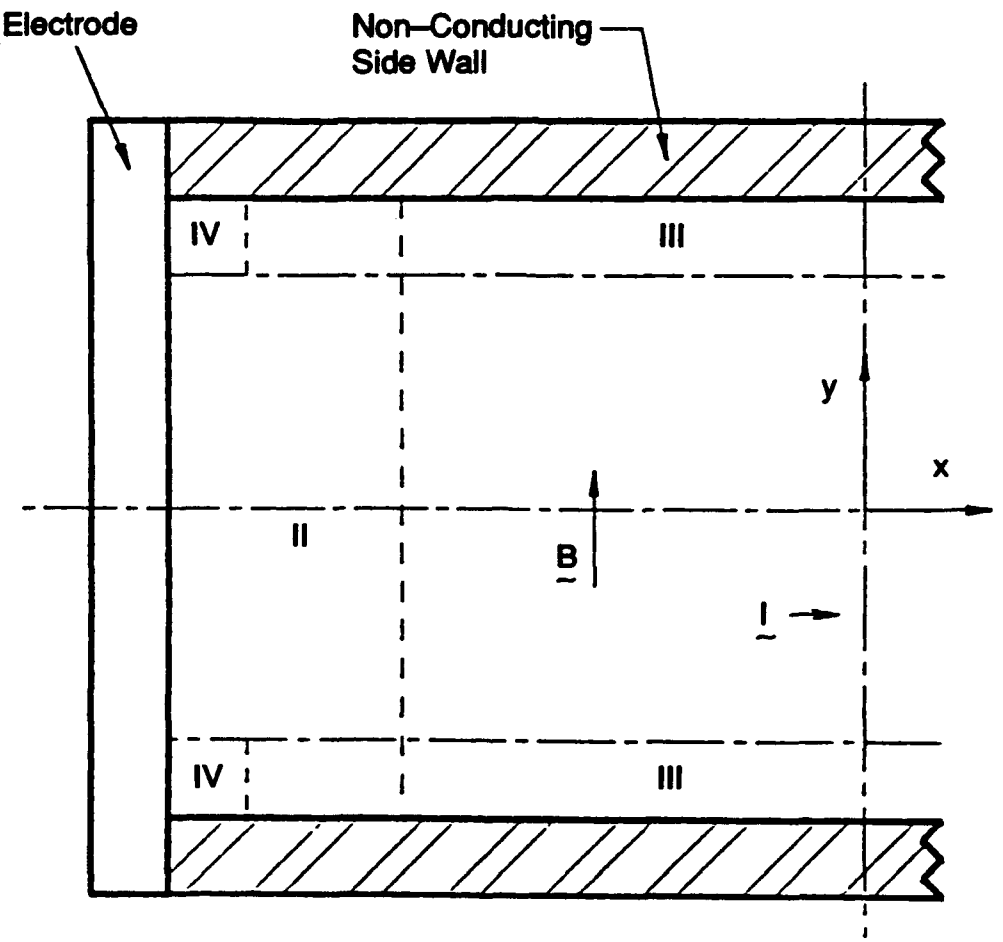

I. Uniform Velocity Core
II. Secondary Boundary Layer O[$M^{-1/2}$]
III. Hartmann Layer O[M^{-1}]
IV. Corner Region O[M^{-1}]

Figure 5. Cross-section of the MHD propulsor drive duct showing the various flow regions.

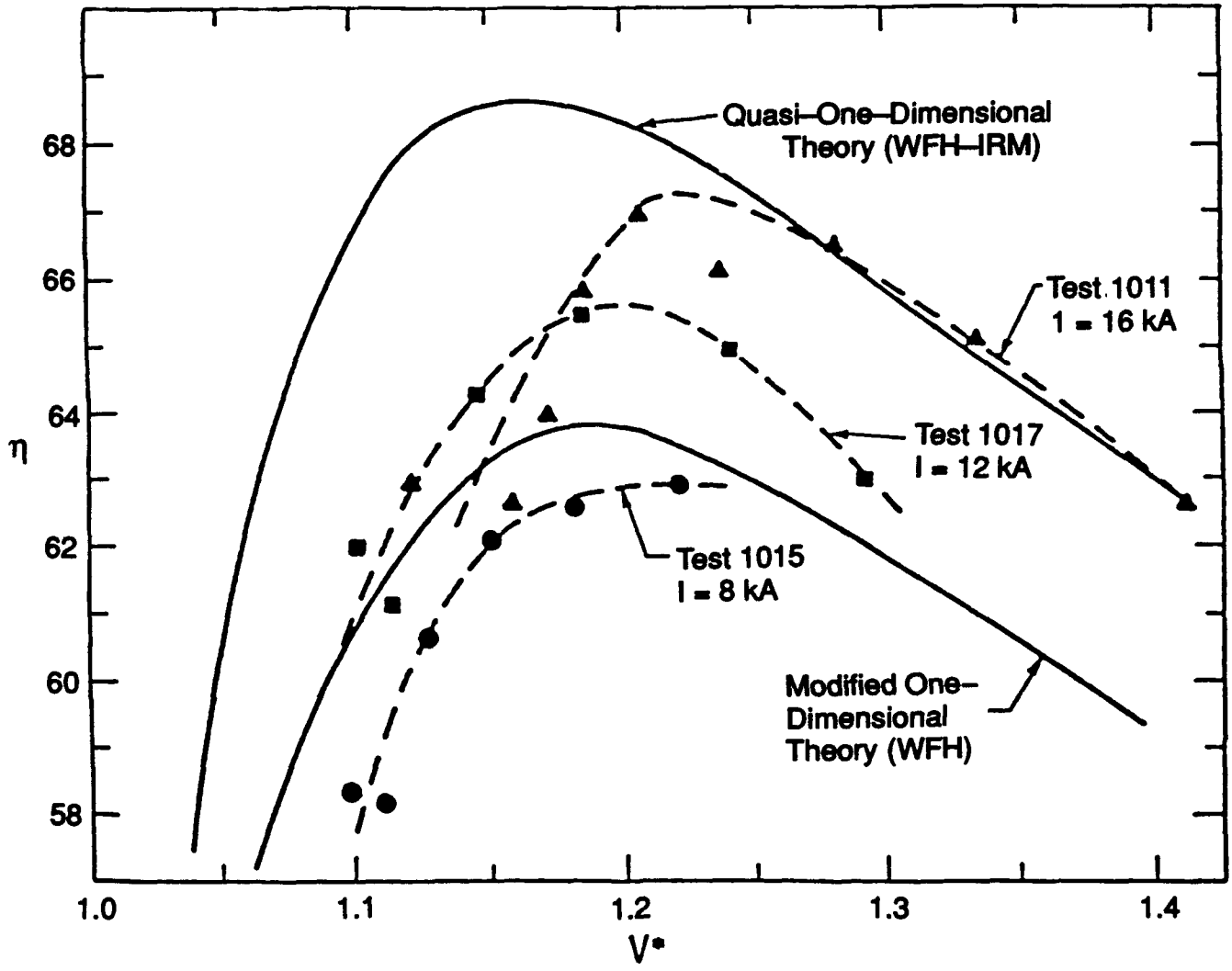

These reported experimental data were obtained using liquid NaK and are compared to their corresponding theoretical results from quasi-one and two dimensional theories of Hughes and McNab[5–8]. The curves represent efficiency η versus dimensionless voltage V*. (Copyrighted material reprinted with permission of AIAA.[9])

Figure 6. Experimental results for MHD duct flows with duct extensions and magnetic field fringing in the end regions.

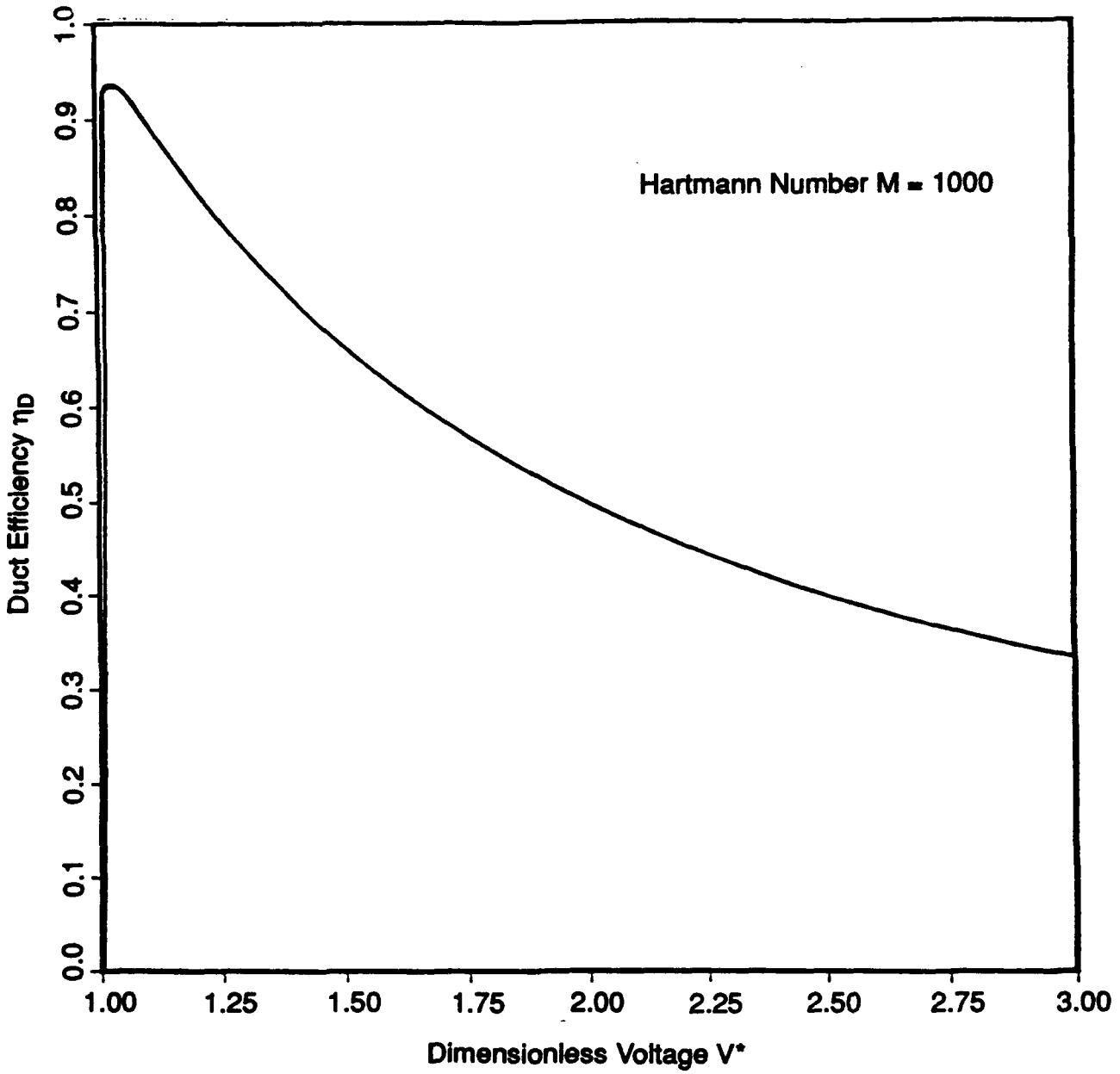

Figure 7. The sensitivity of uniform-field, fully-developed duct efficiency to the variation of dimensionless voltage for typical operating parameters.

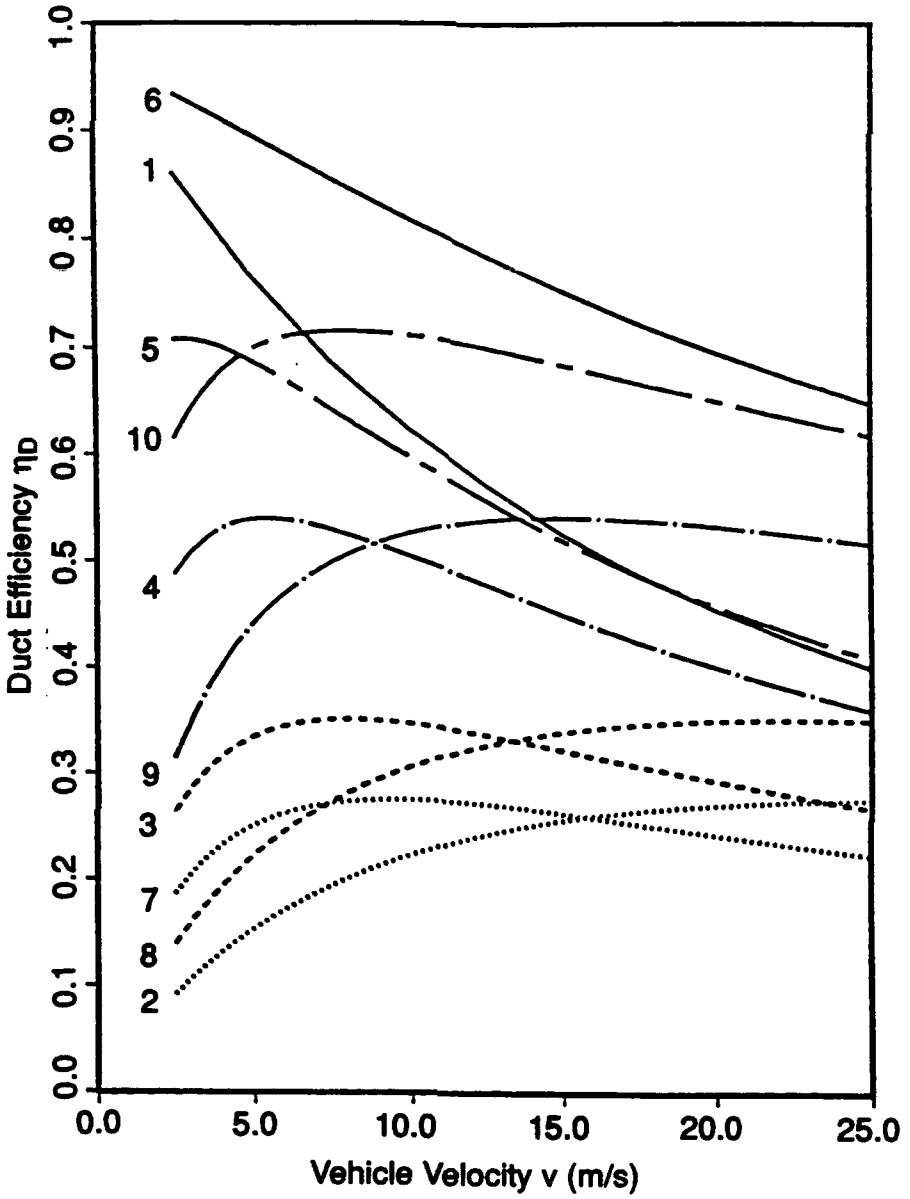

Figure 8. Duct efficiency (mechanical power output to fluid/electrical power input to duct terminals) as a function of vehicle speed and applied magnetic field for a nominal case where:

L = 10.0 m		ρ = 1.03×10^3 kg/m^3	
a = 2.00 m		μ = 1.00×10^{-3} N-s/m	
b = 2.00 *m*		σ = 4.00 S/m	
K = 1500		τ = 6.00 (CASE 4)	

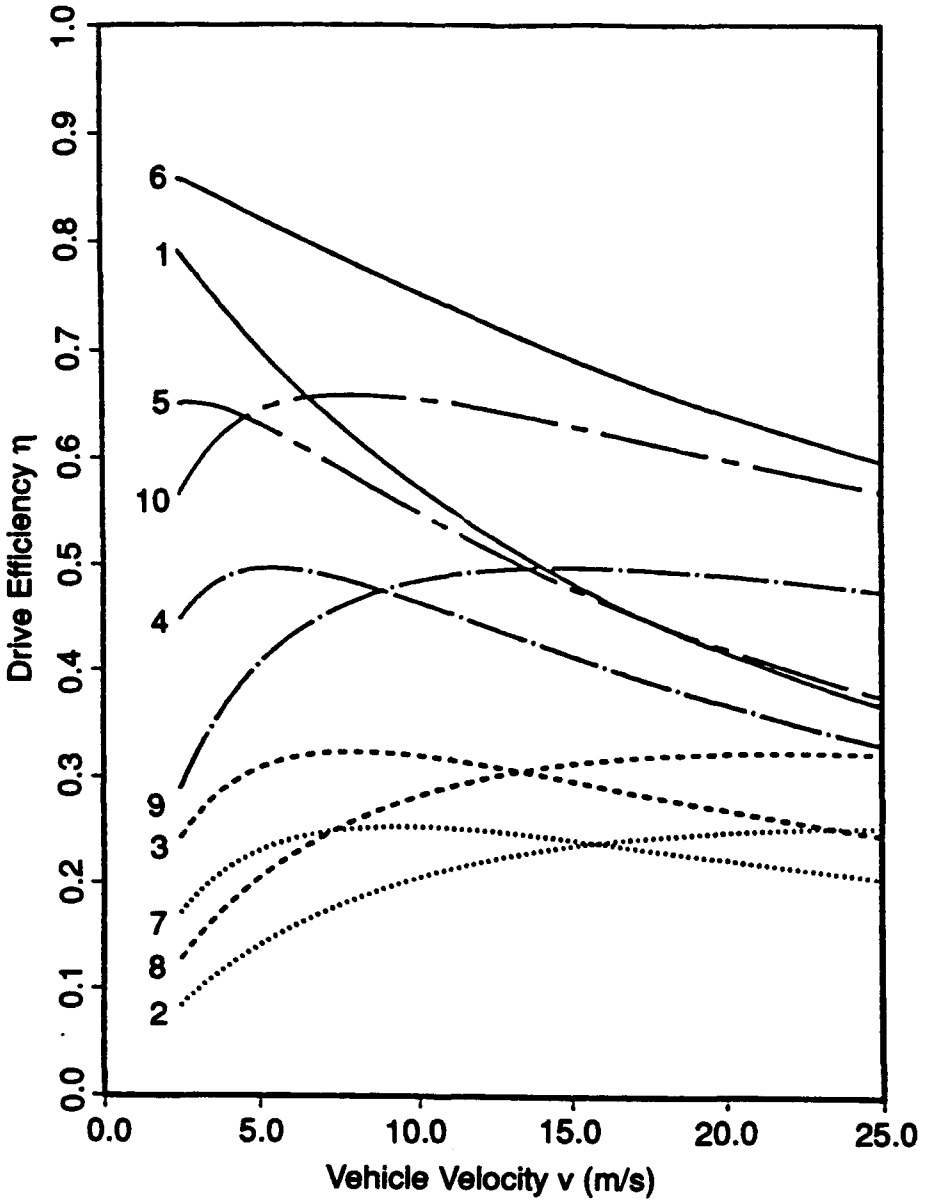

Figure 9. Drive efficiency (vehicle driving power/electrical power input to duct terminals) as a function of vehicle speed and applied magnetic field for a nominal case where:

L	= 10.0 m	ρ	= 1.03×10^{3} kg m^{-3}
a	= 2.00 m	μ	= 1.00×10^{-3} N-s/m
b	= 2.00 m	σ	= 4.00 S/m
K	= 1500	τ	= 6.00 (CASE 4)

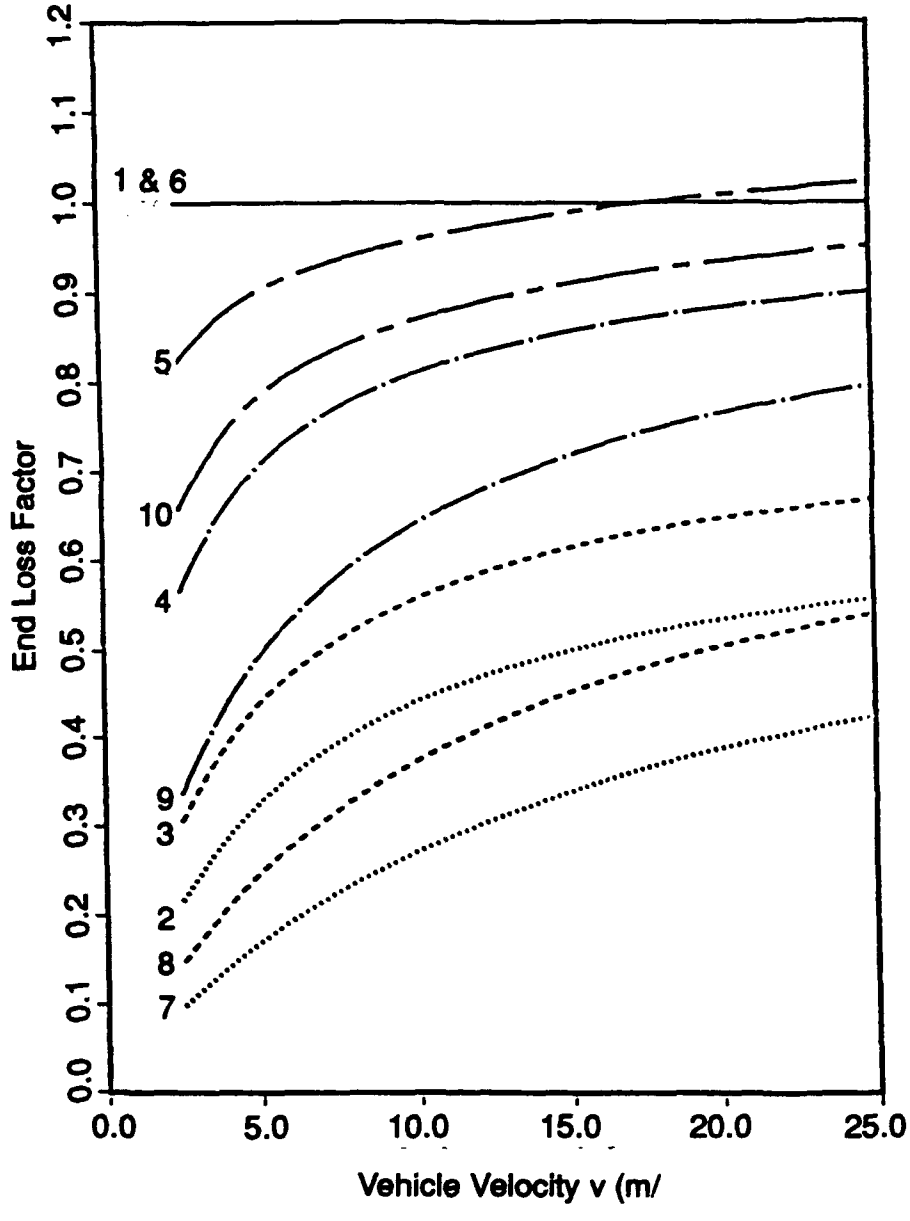

Figure 10. End loss factor (required power input for unit design case of interest/required power for unit with no end losses) as a function of vehicle speed and applied magnetic field for a nominal case where:

L = 10.0 m		ρ = 1.03×10^{3} kg/m^3	
a = 2.00 m		μ = 1.00×10^{-3} N-s/m	
b = 2.00 m		σ = 4.00 S/m	
K = 1500		τ = 6.00 (CASE 4)	

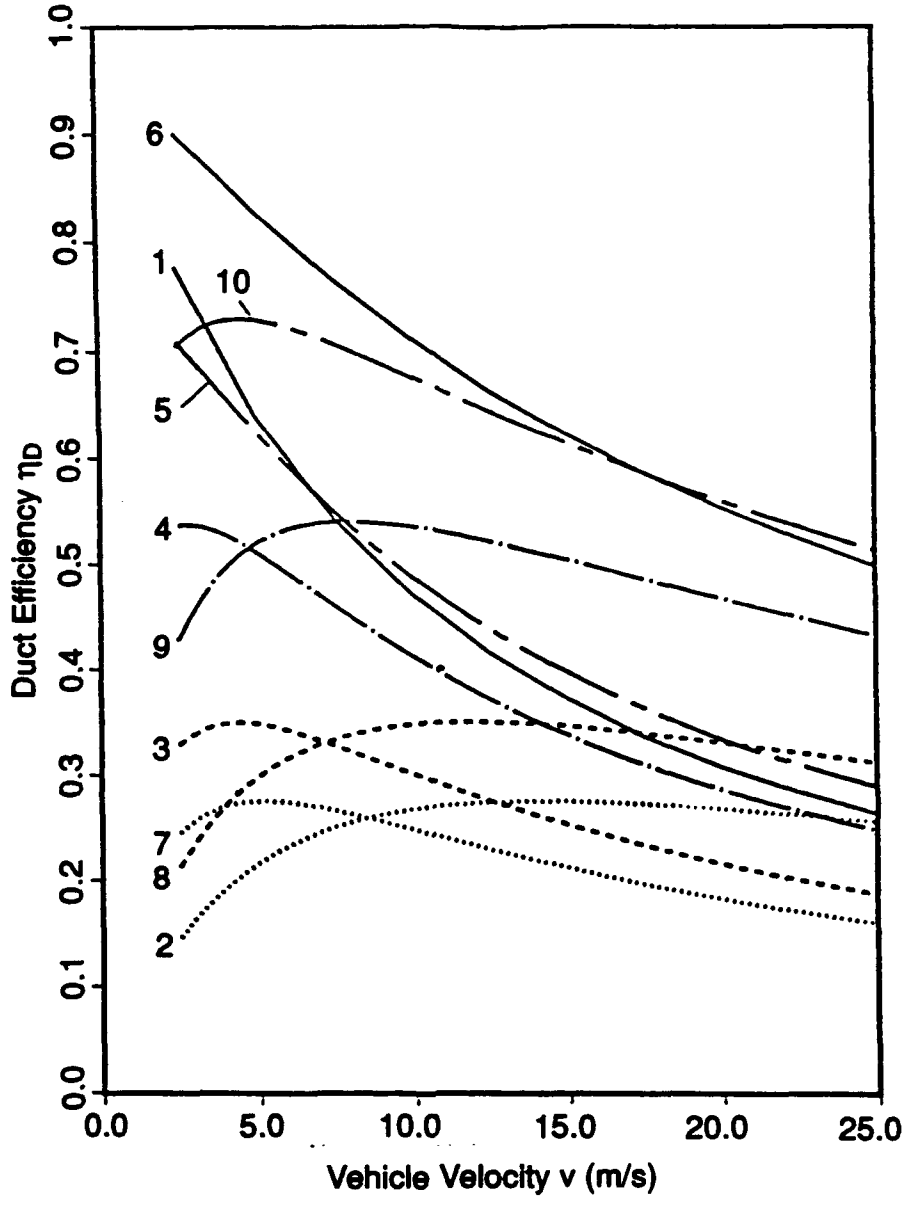

Figure 11. Duct efficiency (mechanical power output to fluid/electrical power input to duct terminals) as a function of vehicle speed and applied magnetic field for a nominal case where:

L	= 10.0 m	ρ	= 1.03×10^3 kg/m^3
a	= 2.00 m	μ	= 1.00×10^{-3} N-s/m
b	= 2.00 m	σ	= 4.00 S/m
K	= 3000	τ	= 6.00 (CASE 4)

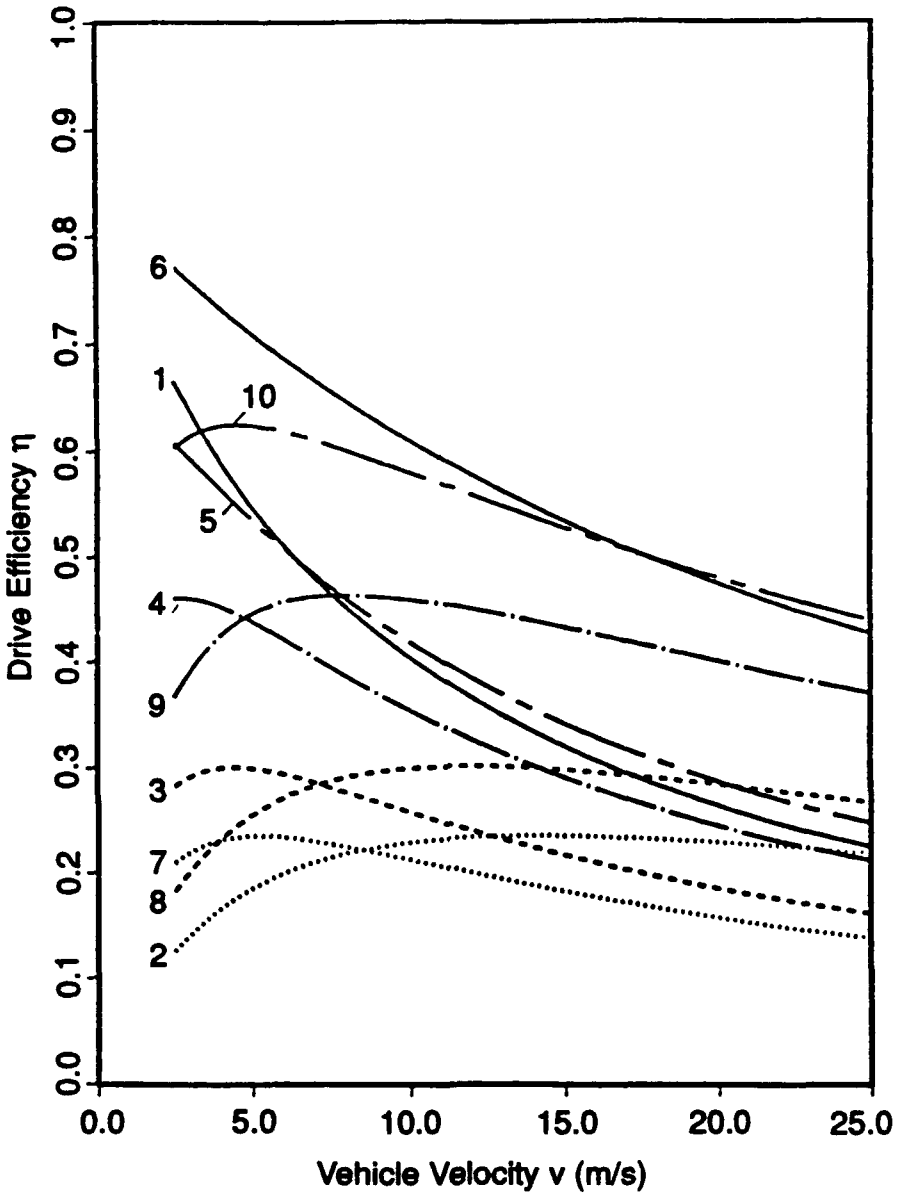

Figure 12. Drive-efficiency (vehicle driving power/electrical power input to duct terminals) as a function of vehicle speed and applied magnetic field for a nominal case where:

L = 10.0 m		ρ = 1.03×10^3 kg/m^3	
a = 2.00 m		μ = 1.00×10^{-3} N-s/m	
b = 2.00 m		σ = 4.00 S/m	
K = 3000		τ = 6.00 (CASE 4)	

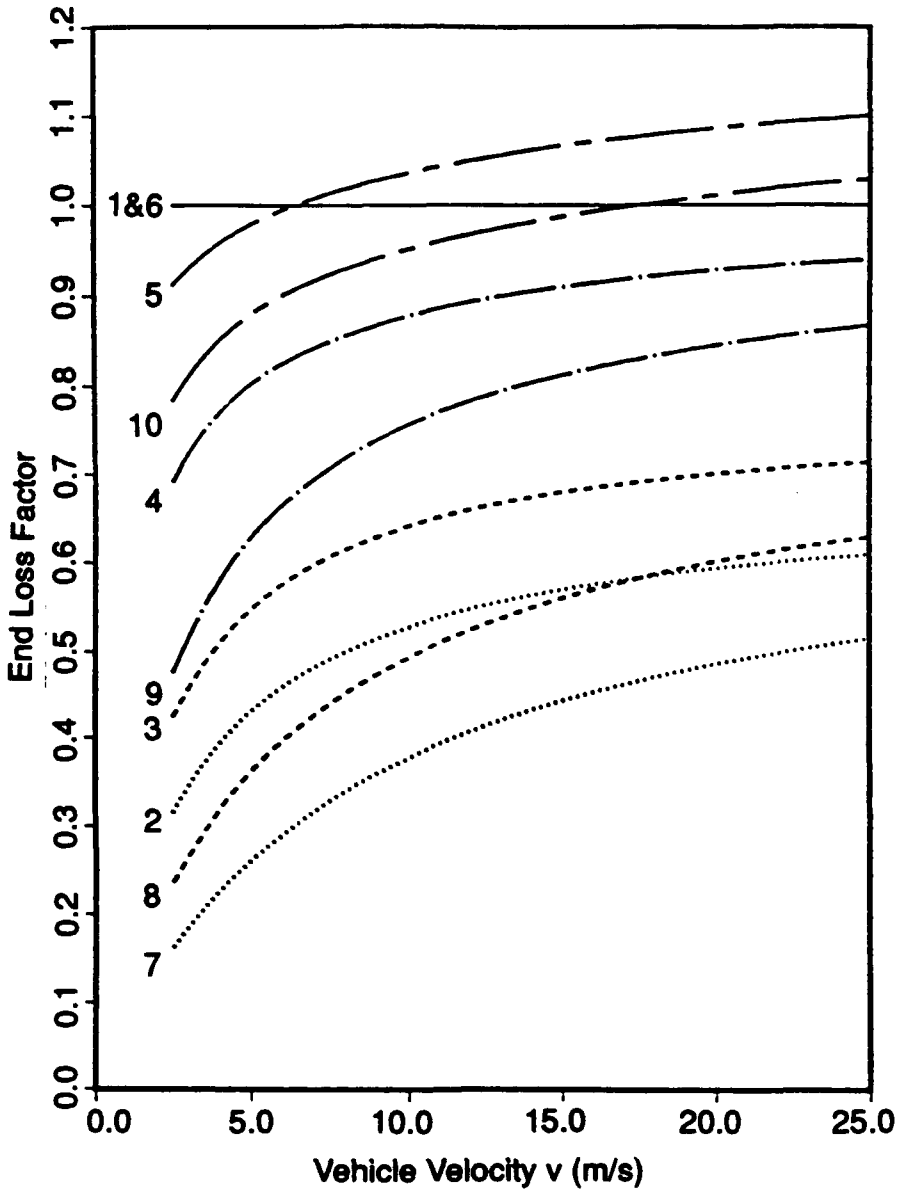

Figure 13. End loss factor (required power input for a unit design case of interest/required power for unit with no end losses) as a function of vehicle speed and applied magnetic field for a nominal case where:

L = 10.0 m		ρ = 1.03×10^3 kg/m^3	
a = 2.00 m		μ = 1.00×10^{-3} N-s/m	
b = 2.00 m		σ = 4.00 S/m	
K = 3000		τ = 6.00 (CASE 4)	

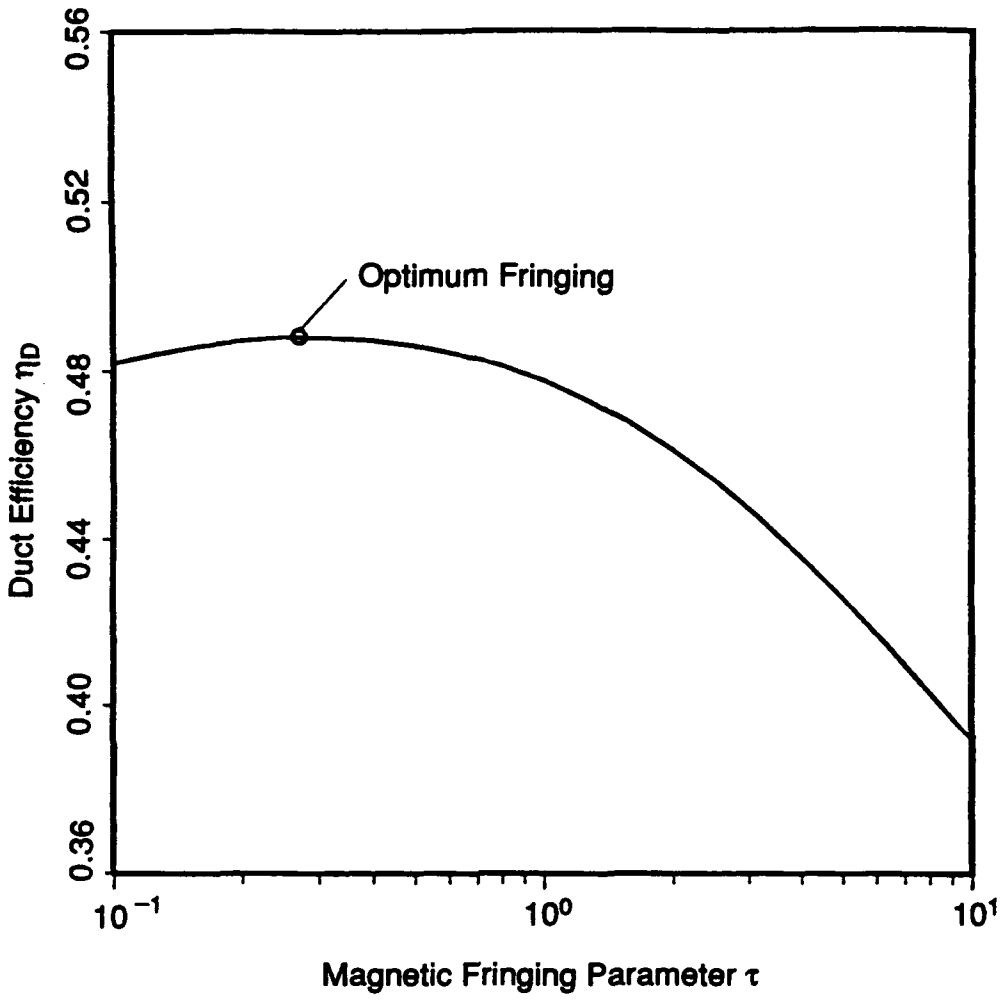

Figure 14. Dependence of duct efficiency on the magnetic fringing parameter for a duct with finite length extensions (Case 4) for a nominal case where:

L	= 10.0 m	μ	= 1.00×10^{-3} N-s/m
a	= 2.00 m	σ	= 4.00 S/m
b	= 2.00 m	B	= 6.00 T
K	= 3000	v	= 10.0 m/s
ρ	= 1.03×10^{3} kg/m^3		

APPENDIX A
COMPUTATIONAL PROCEDURES DEVELOPED FOR DETERMINING THE EXTERIOR CURRENT DISTRIBUTIONS FOR THE CASE 2, MHD PROPULSIVE DUCT

The equations, describing the exterior current distribution for a MHD propulsor with no duct extensions which allows current to fringe into the open sea were derived in the text of this technical report (see equations 21). These equations cannot be solved analytically. The computational procedures set up for solving equations (21) are presented in this appendix.

The source plane is broken into discrete cells and the problem will be solved numerically. Figure A–1 shows the discretized source plane in which test points are located in the geometric center of each cell. There are m cells in a horizontal row and n cells in a vertical column. All the cells are identical in size and shape with physical dimensions $\Delta x'^*$ by $\Delta y'^*$. The indices i and j denote the horizontal and vertical mesh location of a current source cell while the indices k and 1 denote the horizontal and vertical mesh location of a test point in this discrete system. In any source cell, the current source distribution is taken to be uniform. The discrete approximation to equation (19) in the text of the report is written for this scheme as:

$$\phi_{kl}{}^* = \frac{1}{8\pi M_o} \sum_{i=1}^{m} \sum_{j=i}^{n} J_{(z)}{}^* \int_{\Delta y'^*} \int_{\Delta x'^*} \frac{dx'^* dy'^*}{\sqrt{\alpha^2 (x^* - x'^*)^2 + (y^* - y'^*)^2}} \qquad \text{(A–1)}$$

considering the entire source plane.

In this formulation, the array of dimensionless electric potentials is a row vector,

$$\phi^* = [\phi^*_{11}, \ \ldots \phi^*_{1n}, \ \ldots \phi^*_{k1} \ \ldots, \phi^*_{kn}, \ \ldots \phi^*_{m1}, \ \ldots \phi^*_{mn}, \ ]$$

while the array of dimensionless current densities is a column vector.

$$J^*_z = [J^*_{(z)11}, \ \ldots J^*_{(z)1n}, \ \ldots J^*_{(z)i1}, \ \ldots \ J^*_{(z)in}, \ \ldots J^*_{(z)m1}, \ \ldots J^*_{(z)mn}, \ ]^T$$

The array G * may be written to relate the dimensionless electric potentials to the dimensionless current sources as

$$\phi^*_{kl} = \frac{1}{M_o} \sum_{i=1}^{m} \sum_{j=1}^{n} G^*_{klij} \ J^*_{(z)ij} \qquad \text{(A–2)}$$

$\underline{G}^*$ is a square matrix of dimensionless influence coefficients with dimension of $(mn)^2$. Comparing equation (A–2) with (A–1), one sees that the element of $\underline{G}^*$ can be expressed as

$$G^*_{klij} = \frac{1}{8\pi} \int_{\Delta y'^*} \int_{\Delta x'^*} \frac{dx'^* dy'^*}{\sqrt{\alpha^2 (x^* - x'^*)^2 + (y^* - y'^*)^2}} \qquad \text{(A–3)}$$

If many computational cells are used, the physical dimensions of one cell are small compared to the size of the entire source plane. This being true, simple but numerically accurate expressions may be written for all the off-diagonal influence matrix elements or

those elements in which the test point is in a cell outside the source cell. Then equation (A–3) reduces to the expression.

$$G^*_{klij} = \frac{1}{8\pi} \frac{\Delta x' * \Delta y' *}{\sqrt{\alpha^2 (x_i^* - x_k^*)^2 + (y_j * - y_l *)^2}} \quad \text{for } i \neq k, \text{ or } j \neq l \quad \text{(A–4)}$$

All the current sources for a particular cell have been lumped into a point source at the cell's center. This approximation effectively replaces the integral of the source over the cell in equation (A–3) with a value numerically close to its mean value. As the number of cells in the source plane increases, the fractional variation of the length of the radius vector between the source points in a cell and the test point becomes smaller and the approximation becomes more accurate.

To calculate the diagonal influence matrix elements, or those elements in which the test points resides within the source cell, the mean value approximation must be abandoned and the actual integral in equation (A–3) must be performed. The area integral over all the sources in a cell is equal to four times the area integral over the first quadrant by symmetry. The diagonal element of the dimensionless influence coefficient matrix may the be written:

$$G^*_{klij} = \frac{1}{2\pi} \int_0^{\frac{\Delta y' *}{2}} \int_0^{\frac{\Delta x' *}{2}} \frac{dx' * dy' *}{\sqrt{\alpha^2 x'^{*2} + y'^{*2}}} \quad \text{for } i = k, \; j = l \qquad \text{(A–5)}$$

Solving this integral gives the defining equation for G^*_{klij}

$$G^*_{klij} = \frac{\Delta x' *}{4\pi} \left\{ \frac{\Delta y' *}{\Delta x' *} \, ARCCSH\left(\frac{\Delta y' *}{\alpha \Delta x' *} \right) + ARCSINH\left(\frac{\Delta y' *}{\alpha \Delta x' *} \right) \right\} \qquad \text{(A–6.1)}$$

Writing the inverse hyperbolic functions above in terms of natural logarithms yields:

$$G^*_{klij} = \frac{\Delta x' *}{4\pi} \left\{ \frac{\Delta y' *}{\Delta x' *} \ln \left[\frac{\alpha \Delta x' *}{\Delta y' *} + \sqrt{1 + \left(\frac{\alpha \Delta x' *}{\Delta y' *} \right)^2} \right] \right. \qquad \text{(A–6.2)}$$

$$\left. + \ln \left[\frac{\Delta y' *}{\alpha \Delta x' *} + \sqrt{1 + \left(\frac{\alpha \Delta x' *}{\Delta y' *} \right)^2} \right] \right\}$$

which readily allows the numerical evaluation of the influence coefficient.

Axes of symmetry and of antisymmetry allow the solution of one quadrant to be reflected into the others which reduces the computational burden. Figure (A–2) shows a current source of strength s in the first quadrant reflected into the other quadrants. Reflecting the source points in both the first and fourth quadrants into the second and third quadrants gives sources of strength – s there. One can now modify the influence coefficients so that electric potentials need be found only in the first quadrant, but where

sources over the entire source plane are contributing. Accounting for the proper sign on the sources and the distance between the source and test points and writing all quantities in dimensionless form, the general form for the off-diagonal dimensionless influence coefficients for the first quadrant is obtained from equation (A–4) and written as

$$G^*_{1klij} = \frac{1}{8\pi} \left\{ \frac{\Delta x'^* \Delta y'^*}{\sqrt{\alpha^2(x_i^* - x_k^*)^2 + (y_j^* - y_l^*)^2}} - \frac{\Delta x'^* \Delta y'^*}{\sqrt{\alpha^2(x_i^* + x_k^*)^2 + (y_j^* - y_l^*)^2}} \right.$$

$$\left. + \frac{\Delta x'^* \Delta y'^*}{\sqrt{\alpha^2(x_i^* - x_k^*)^2 + (y_j^* - y_l^*)^2}} - \frac{\Delta x'^* \Delta y'^*}{\sqrt{\alpha^2(x_i^* + x_k^*)^2 + (y_j^* - y_l^*)^2}} \right\} \text{(A–7)}$$

for $i \neq k$, or $j \neq l$

$\underline{G}_1{}^*$ is a modified influence coefficient matrix for the first quadrant only. Consequently, all the indices are now assumed to pertain only to the first quadrant.

For a diagonal element in the first quadrant, the general form considering all current sources may be obtained with the use of equations (A–4) and (A–6.2). The diagonal element may be written:

$$G^*_{1klij} = \frac{1}{16\pi} \left\{ \frac{-\Delta x'^* \Delta y'^*}{a x_i^*} + \frac{\Delta x'^* \Delta y'^*}{y_j^*} - \frac{\Delta x'^* \Delta y'^*}{\sqrt{\alpha^2 x_i^{*\,2} + y_j^{*\,2}}} \right.$$

$$+ 4\Delta x'^* \left(\frac{\Delta y'^*}{\Delta x'^*}\right) \ln\left[\frac{\alpha \Delta x'^*}{\Delta y'^*} + \sqrt{1 + \left(\frac{\alpha \Delta x'^*}{\Delta y'^*}\right)^2}\right]$$

$$\left. + \ln\left[\frac{\Delta y'^*}{\alpha \Delta x'^*} + \sqrt{1 + \left(\frac{\Delta y'^*}{\Delta x'^*}\right)^2}\right] \right\} \text{ for } i = k \text{ or } j = l \text{ (A–8)}$$

Given a computational mesh, all the elements of the influence coefficient matrix may be found for the electric potentials in the first quadrant. The influence coefficient matrix may be inverted and the current densities for each cell in the first quadrant may be found from

$$J^*_{(z)ij} = \sum_{k=1}^{m} \sum_{l=1}^{n} M_o G^{*\,-1}_{1ijkl} \phi^*_{kl} \qquad \text{(A–9)}$$

where the nodal values of ϕ^*_{kl} are specified by relation $\phi^* = -\frac{1}{2} V^* x^*$, and the elements $\underline{G}_1{}^*$ are given by equation (A–7) or equation (A–8).

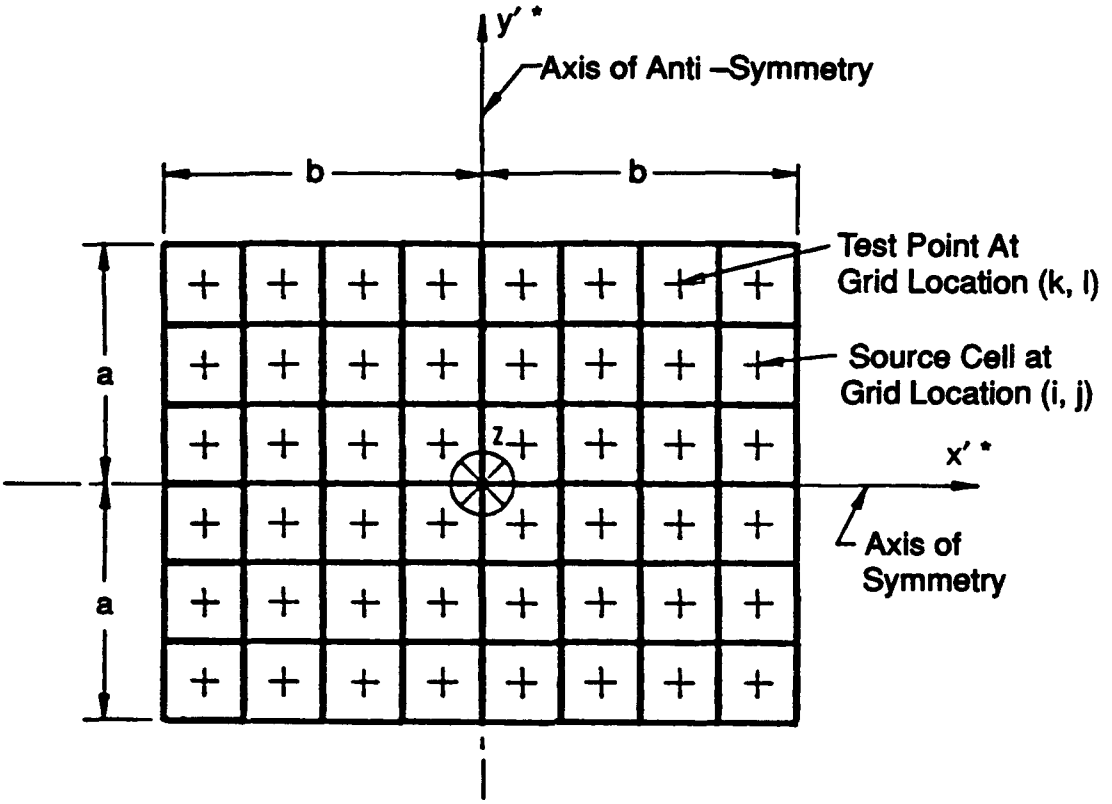

Figure A–1. Discretization of the current source rectangle for the approximate solution to the governing integral equation for the total fringing current. Mesh is m cells wide and n cells tall. Cell dimensional are $\Delta x'^*$ by $\Delta y'^*$

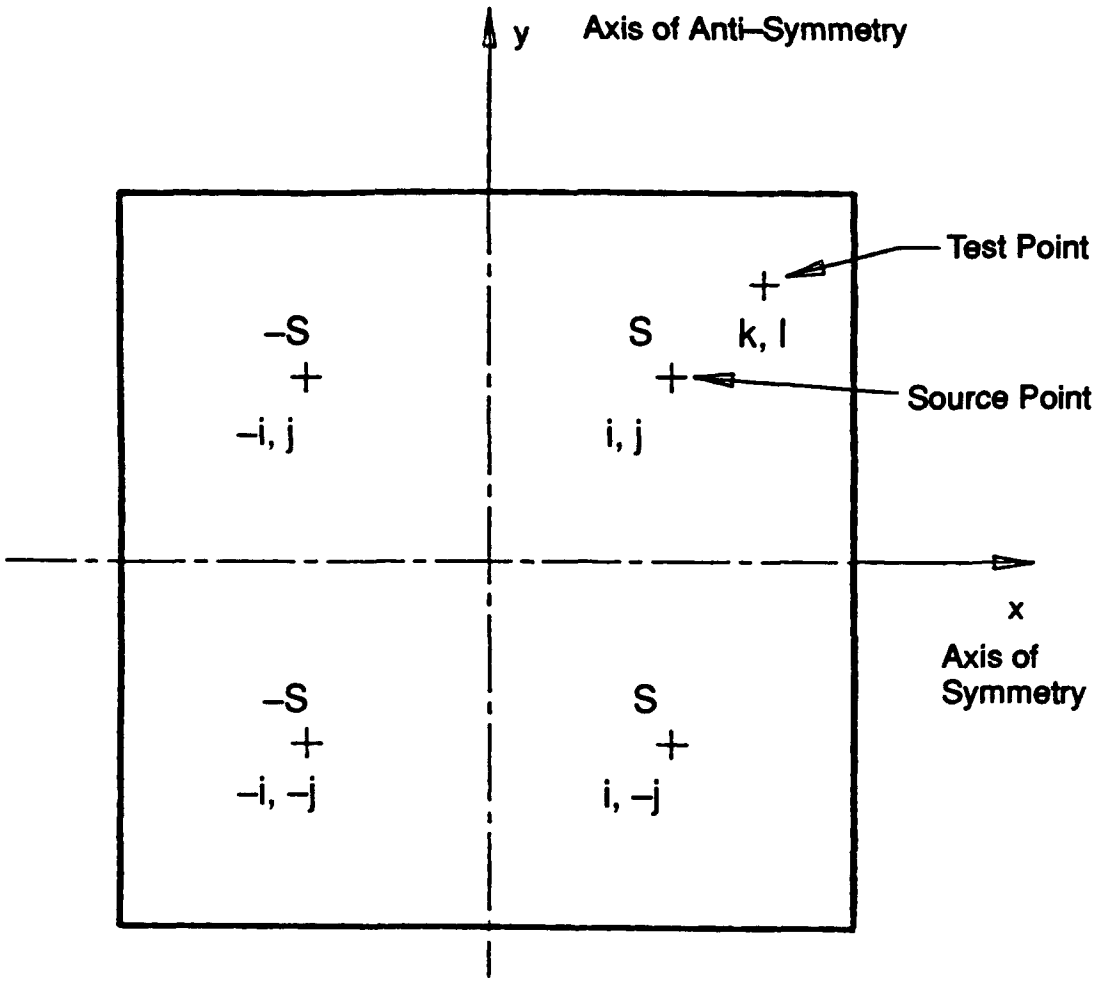

Figure A–2. Symmetric and anti-symmetric reflections of a current source point of the first quadrant in the Green's function solution technique. The mesh location of the test point is (kl) and the mesh location of the source point of strength s is (i, j).

REFERENCES

1. Brown, S.H., J.S. Walker, N.A. Sondergaard, J.P. Reilly, and D.E. Bagley, "Propulsive Efficiencies of Magnetohydrodynamic Submerged Vehicular Propulsors," United States Navy Report DTRC–90/009, David Taylor Research Center, Bethesda, Maryland (April 1990).

2. Bewley, L.V., *Two-Dimensional Fields in Electrical Engineering*, p. 142, Dover Publishing, New York, New York (1963).

3. Hunt, J.C.R., "Magnetohydrodynamic Flow in Rectangular Ducts," *J. Fluid Mech.*, 21, pp. 577–590 (1965).

4. Hunt, J.C.R. and K. Stewartson, "Magnetohydrodynamic Flow in Rectangular Ducts II," *J. Fluid Mech.*, 23, pp. 563–581 (1965).

5. Hughes, W.F. and I.R. McNab, "A Quasi-One-Dimensional Analysis of an Electromagnetic Pump Including End Effects," *Liquid-Metal Flows and Magnetohydrodynamics*, H. Branover, A. Yakot, and P. S. Lykoudis eds., vol. 84 *Progress in Astronautics and Aeronautics*, pp. 287–312 (May 1983).

6. Hughes, W.F. and C.C. Alexion, "A Theoretical Analysis of the DC Electromagnetic Flow Coupler," *Nuclear Engineering and Design*, vol. 74, pp. 367–376 (March 1983).

7. NSF Final Report by W.F. Hughes (Principal Investigator), I.R. McNab, C.C. Alexion, A.R. Keeton, and P.A. Ciarelli, Carnegie Mellon University, Pittsburgh, Pennsylvania, "Industry/University Cooperative Program: High Interaction Parameter Magnetohydrodynamic Studies of Liquid Metal Flows," NSF Grant No. ENG–78–08734 (October 1981).

8. NSF Final Report by W.F. Hughes (Principal Investigator), Carnegie Mellon University, Pittsburgh, Pennsylvania, "Industry/University Cooperative Program: Finite Element Methods and Approximate Analytical Studies in Liquid-Metal MHD Flows," NSF Grant No. CPE–8108952 (May 1, 1984).

9. Alexion, C.C. and Keeton, A.R., "Experiments on a Large Thin-Wall Duct," Progress in Astronautics and Aeronautics, Vol 100 (1985), Single and Multiphase Flows in Electromagnetic Field, Edited by H. Branover, P.S. Lykoudis, and M. Mond.

10. NSF Final Report by C.C. Alexion (Principal Invest[illegible]), Westinghouse R and D Center, Pittsburgh, Pennsylvania, "Industry-Univer[illegible]operative Program: High Interaction Parameter Magnetohydrodynamic Studies in Liquid Metal Flows" (December 31, 1984).

11. Nathenson, R.D., C.C. Alexion, A.R. Keeton, and D.E. Gray, "Demonstration of Flow Coupler for LMFBRs: Single and Multi-Phase Flows in an Electromagnetic Field-Energy, Metallurgical, and Solar Applications," *Progress in Astronautics and Aeronautics*, vol. 100, AIAA, p. 553 (1983).

12. Press, W.H., B.P Flannery, S.A. Teukolsky, and W.T. Vetterling, *Numerical Recipes: The Art of Scientific Computing*, Cambridge University Press, Cambridge, England pp. 31–38 and pp. 294–300 (1986).

INITIAL DISTRIBUTION

Copies

2 James Gagorik

2 Gene Remers

2 Richard Martin
Office of Chief of Naval Research
Office of Naval Technology
800 N. Quincy St.
Arlington, VA 22217–5000

1 Capt. Charles B. Young
Advanded Technology

3 Dr. Robert Rosenfeld
Undersea Warfare Office
DARPA
1555 Wilson Blvd.
Arlington, VA 22209

2 Capt. Davis

2 John M. Sofia
NAVSEA (SEA 92R)

12 DTIC

10 Dr. William H. Hughes
Carnegie Mellon University
Mechanical Engineering
Pittsburgh, PA 15213

2 Dr. John S. Walker
University of Illinois at Urbana–Champaign
Rept. Mechanical & Ind. Eng.
144 Mechanical Engineering Blvd.
1206 West Green St.
Urbana, IL 61801

2 Dr. Daniel W. Swallom
Textron Defense Systems
2385 Revere Beach Parkway
Everett, MA 02149

2 Dr. Michael Petrick
Argonne National Laboratory
9700 South Case Ave.
Argonne, Il 60439

1 Dr. Kenneth E. Tempelmeyer
C/O Office of the Dean College of Engineering and Technology
Southern Illinois University
Carbondate, IL 62901

2 Dr. Basil Picologlow
Engineering Physics Division
Argonne National Laboratory
9700 South Case Ave.
Argonne, IL 60439

CENTER DISTRIBUTION

Copies	Code	Name
2	01	Richard E. Metry
1	0113	Dr. Bruce E. Douglas
1	15	
1	154	Justin H. McCarthy
1	1561	Geoffrey Cox
1	19	
1	1903	
2	1942	Dr. T. M. Farabee
1	27	
3	271	Howard O. Stevens
2	2711	David E. Bagley
1	2711	Robert C. Smith
5	2712	Dr. Samuel H. Brown
5	2712	Dr. N. A. Sondergaard
2	2712	Michael J. Superczynski
1	272	
2	274	
1	3421	TIC Carderock
2	3422	TIC Annapolis

REPORT DOCUMENTATION PAGE

Form Approved
OMB No. 0704-0188

Public reporting burden for this collection of information is estimated to average 1 hour per response, including the time for reviewing instructions, searching existing data sources, gathering and maintaining the data needed, and completing and reviewing the collection of information. Send comments regarding this burden estimate or any other aspect of this collection of information, including suggestions for reducing this burden, to Washington Headquarters Services, Directorate for Information Operations and Reports, 1215 Jefferson Davis Highway, Suite 1204, Arlington, VA 22202-4302, and to the Office of Management and Budget, Paperwork Reduction Project (0704-0188), Washington, DC 20503.

1. AGENCY USE ONLY *(Leave blank)*	2. REPORT DATE	3. REPORT TYPE AND DATES COVERED
	April 1992	

4. TITLE AND SUBTITLE
Propulsion Efficiencies of Magnetohydrodynamic Propulsors Considering Electrical and Magnetic End Effects

5. FUNDING NUMBERS
Program ElementNo. 62121N
Task Area R2146HOE
Work UnitNo. 1–2712–120

6. AUTHOR(S)
Paul A. Beatty, William F. Hughes, Samuel H. Brown, Joseph D. Walters, Neal A. Sondergaard, and Howard O. Stevens

7. PERFORMING ORGANIZATION NAME(S) AND ADDRESS(ES)
Annapolis Detachment
Carderock Division
Naval Surface Warfare Center
Annapolis, MD 21402

8. PERFORMING ORGANIZATION REPORT NUMBER
CDNSWC–92/004

9. SPONSORING /MONITORING AGENCY NAME(S) AND ADDRESS(ES)
Office of Naval Technology
ONT–211 (Gagorik, James
800 N. Quincy St.
Arlington, VA 22217–5000

10. SPONSORING /MONITORING AGENCY REPORT NUMBER

11. SUPPLEMENTARY NOTES

12a. DISTRIBUTION /AVAILABILITY STATEMENT
Approved for public release; distribution is unlimited.

12b. DISTRIBUTION CODE

13. ABSTRACT *(Maximum 200 words)*

A mathematical theory for the performance of a direct current, rectangular duct magnetohydrodynamic (MHD) propulsion system propelling a marine vehicle is presented. The model accounts for the effects of spatially nonuniform magnetic fields and current distributions which are present at the ends of the propulsion unit. The theory is based on an approximate solution of the general MHD duct flow problem in which the mutual interaction of the electric current and fluid flow in a strong magnetic field are considered in detail. For a specified vehicular steady state cruising speed, the propulsive efficiency and electrical power requirements can be calculated from the theory given the hydrodynamic drag of the vehicle and the properties of the fluid medium. Explicit electrical end loss factors are calculated to relate the performance of a propulsor with nonuniform field distributions to the performance of an idealized propulsor with no end losses operating under the same conditions. The power losses due to auxiliary equipment such as electrical generators, buswork, and magnetic cryogenic systems are not included in the study.

Numerical results from the models for five design configurations for a nominal geometry under a reasonable range of operating parameters are presented. The numerical results, including the ideal propulsor with no end effects, indicate that the fringing magnetic and current distributions at the ends of the duct generally significantly degrade the propulsive efficiency. The degree of degradation depends on details of the design configuration of the rectangular duct.

14. SUBJECT TERMS			15. NUMBER OF PAGES
			16. PRICE CODE
17. SECURITY CLASSIFICATION OF REPORT	18. SECURITY CLASSIFICATION OF THIS PAGE	19. SECURITY CLASSIFICATION OF ABSTRACT	20. LIMITATION OF ABSTRACT
UNCLASSIFIED	UNCLASSIFIED	UNCLASSIFIED	